

phys. stat. sol. (b) **192**, 407 (1995)

Subject classification: 68.35 and 68.45; 73.20; S10.1

Physical Chemistry I, Ruhr-University Bochum¹⁾

Metal Oxide Surfaces: Electronic Structure and Molecular Adsorption

By

H.-J. FREUND

(Received September 11, 1995)

The surface science of oxides has received considerably less attention than the study of metal surfaces. We review some of our work on structural characterization and electronic structure investigations on oxide surfaces which we prepare as thin oxide films on metallic substrates. This preparation method leads to certain experimental advantages concerning the application of electron spectroscopies on such systems. We discuss molecular adsorption on non-polar and polar surfaces of clean oxides. The influence of metal deposition onto the oxide surfaces and on their properties with respect to adsorption is described. Light induced processes with full quantum state detection of desorbing molecules are addressed. The possibility of studying dynamic processes in adsorbates on oxides via electron spin resonance spectroscopy is evaluated.

1. Introduction

The last thirty years of surface science have seen an enormous development [1]. The investigations on clean, well structured metal surfaces have contributed to this development considerably [2, 3]. Other types of surfaces have played a much less important role. This is somewhat surprising, because, although there is no doubt about the importance of metals in heterogeneous catalysis, it is clear that in catalysis oxide surfaces are at least as central. An increasing number of groups have, therefore, started to investigate oxide surfaces with respect to geometric and electronic structure as well as molecular adsorption [4 to 6]. We address in the present paper some aspects of the surface science of oxide surfaces.

Specific aspects include:

- surface states on oxide surfaces and their relation to the geometric structure of the surface as well as their modification by molecular adsorption;
- modification of oxide surfaces by metal deposits and its influence on the adsorption behaviour as studied by surface science techniques;
- molecular motion in adsorbates as studied by magnetic resonance.

2. Experimental Aspects

The experiments are performed in ultrahigh vacuum chambers which are equipped with preparation sections. There are several techniques that are used to prepare the oxide surfaces. Oxide surfaces may be prepared by cleavage of bulk samples or via the creation of thin films. Fig. 1 summarizes the possibilities for oxide preparation. So-called nonpolar (100)

¹⁾ D-44780 Bochum, Federal Republic of Germany.

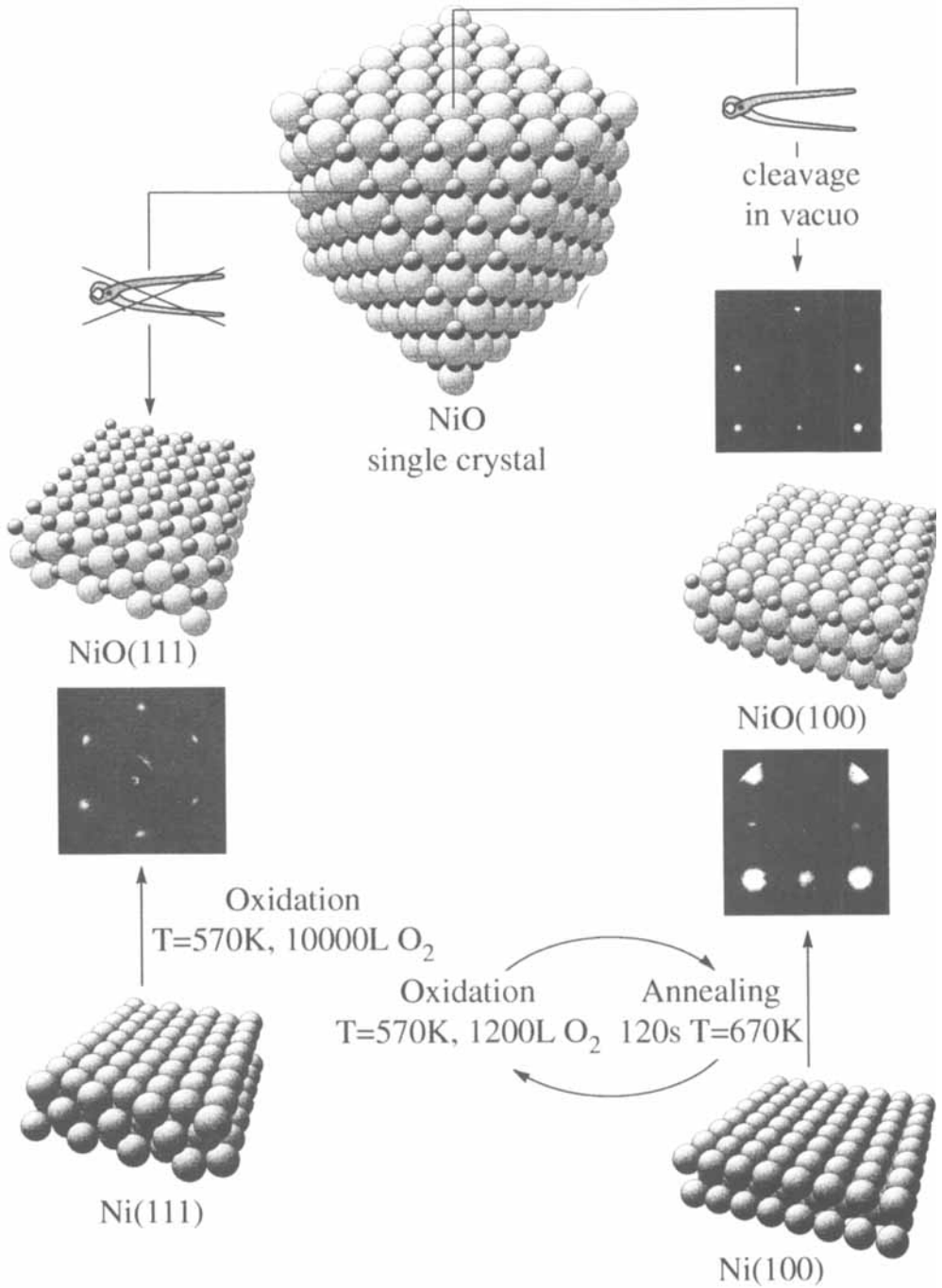


Fig. 1. Summary of preparation methods for oxide samples using the example of NiO

surfaces may be created via cleavage (pliers symbol) leading to high-quality LEED patterns. The same surfaces may be created either via oxidation of a Ni(100) substrate [7, 8]. In this case a LEED pattern with broad spots is observed indicating the presence of defects partly induced by the large lattice mismatch between Ni and NiO. A LEED pattern of single crystal cleavage quality is found for NiO films with nonpolar orientation grown on top of an inert Ag(100) substrate [9]. In other words, the thin film techniques give us to a certain degree control over the defect density in the oxide. Furthermore, this technique allows the growth of polar oxide surfaces which are not available via cleavage of bulk samples [10, 11]. The LEED patterns are of relatively high quality even when grown on a Ni substrate. We employ electron spectroscopic methods such as UPS, XPS, AES, ELS, HREELS, and STM, LEED, SEM, distributed over a number of instruments.

3. Surface States on Oxide Surfaces

We shall start the discussion on oxide surfaces with the stable, nonpolar (100) surfaces of NiO [12] and CoO [13].

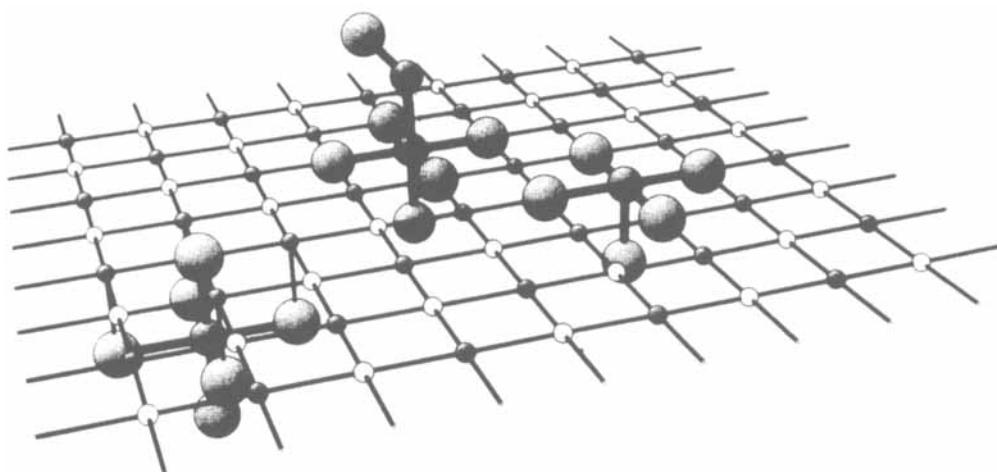
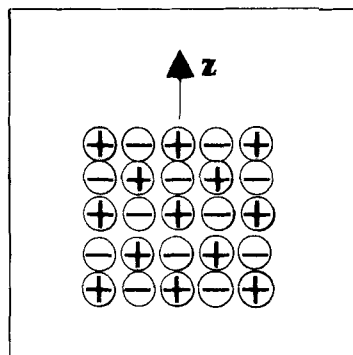


Fig. 2. Schematic representation of the coordination of Ni ions in the bulk, at the clean surface, and at the molecule covered surface

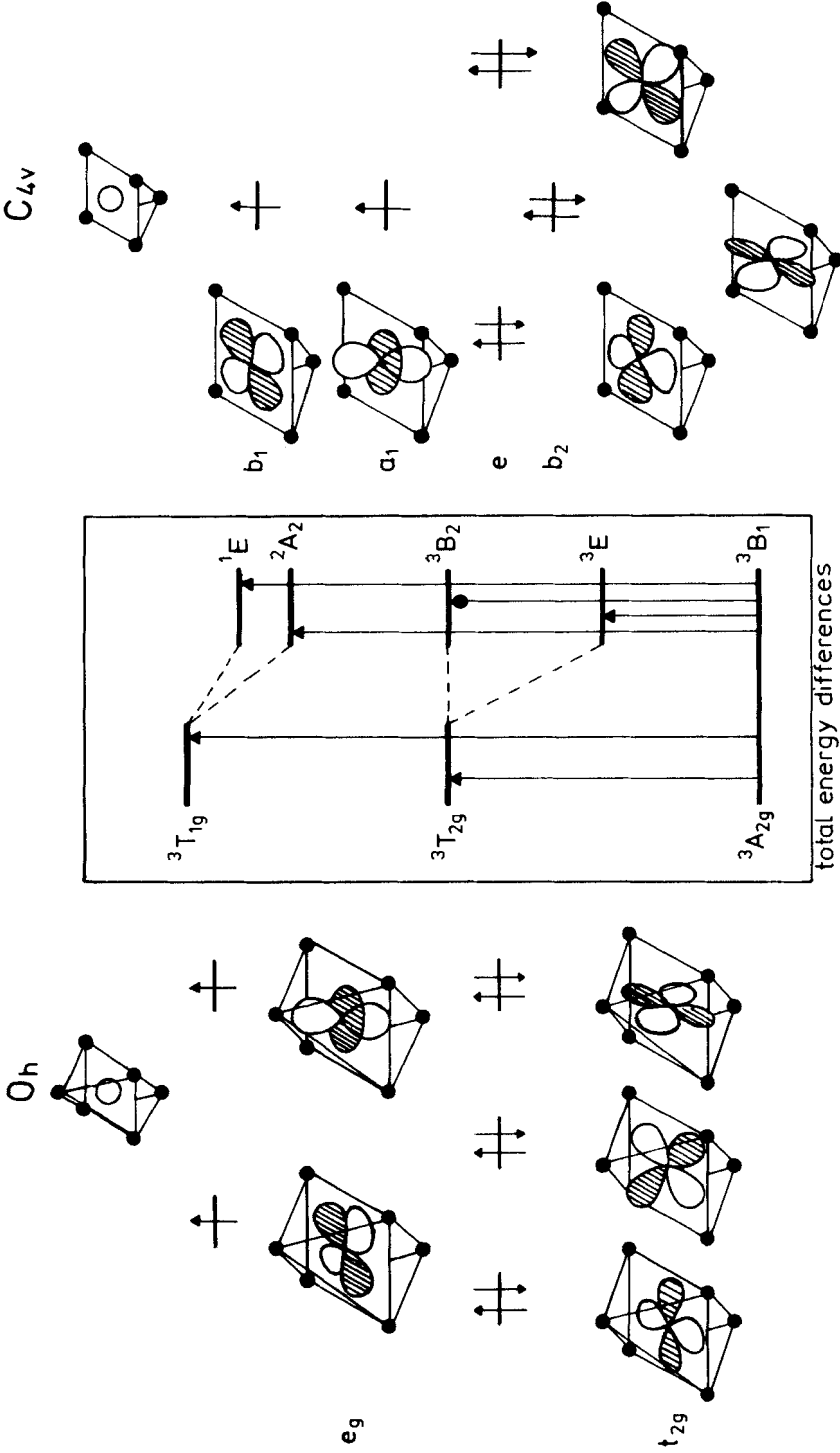


Fig. 3. Shapes and energies of the d-orbitals in NiO in the bulk (O_h) and at the surface (C_{4v}). The excitation energies as calculated via ab-initio calculations by Freitag et al. [12] are shown in the middle panel

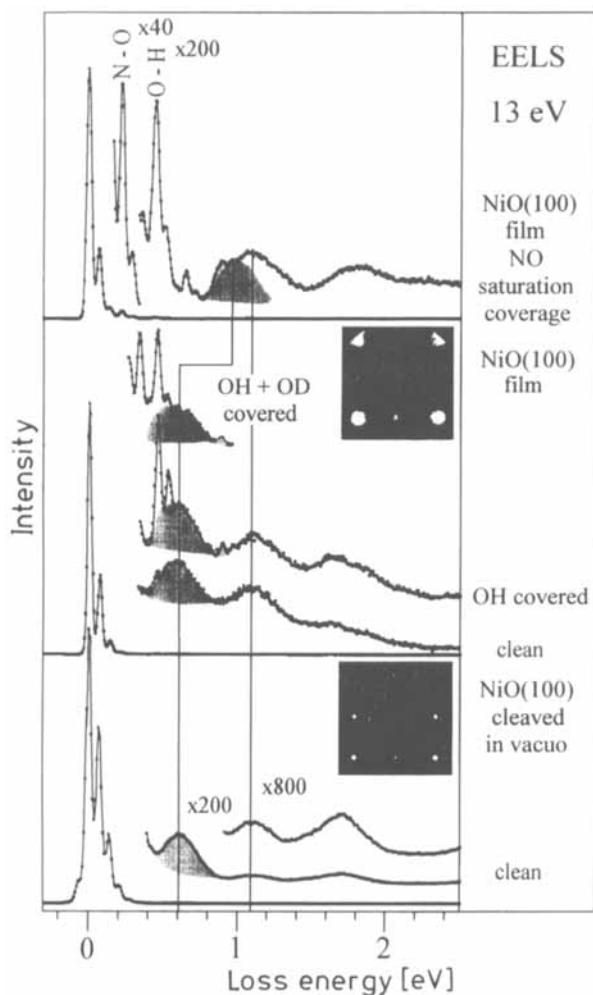


Fig. 4. Electron energy loss spectra of NiO(100) for the clean cleaved NiO(100) surface (bottom) as well as for the OH contaminated NiO(100) film (middle), and the NO covered NiO(100) film (top)

The question is: Can we observe surface specific effects which are connected to the fact that the atoms in the surface are not fully coordinated as compared with the atoms in the bulk of the crystal? Fig. 2 illustrates the octahedral coordination in the bulk and compares it with the fivefold coordination in the surface layer. It is now quite obvious that we would have to look for ligand field effects [12]. Those will be most pronounced for the Ni ions

with their unfilled d-shell. We consider the situation for the d-orbitals in more detail in Fig. 3. Briefly, an octahedral field splits the d-orbitals in a threefold degenerate t_{2g} - and a twofold degenerate e_g -set. Ni^{2+} carries eight electrons, six occupying the t_{2g} -set and two unpaired electrons the e_g -set. This leads to a ${}^3A_{2g}$ state. The two lowest-lying excited states in this octahedral field are of ${}^3T_{2g}$ and ${}^3T_{1g}$ type and are situated at 1 and 1.81 eV, respectively. If we reduce the ligand field by taking one of the ligands off the symmetry as well as the repulsion is reduced and this splits the t_{2g} -set into an e - and a b_2 -component, and the e_g -set into an a_1 - and a b_1 -component. At the same time the splitting in the d-levels is reduced and the excited states shift to lower energy and are increased in number. Therefore, it should in principle be possible to observe these shifts in an electronic excitation spectrum. We can detect these electronic excitations with electron energy loss spectroscopy. Fig. 4 shows the EL- spectra of a clean cleaved NiO(100) surface [12]. The assignment of the states is given in the figure. Even without a detailed assignment, which has been discussed by Freitag et al. [12], it is obvious that the lowest-lying state is localized in the NiO surface.

The d-d excitations are located in the band gap region below the onset of the charge transfer excitations across the band gap. Very similar excitations as observed at the cleaved surface are found at the surface of a thin film (second lowest trace) as indicated in Fig. 4. The other spectra included in Fig. 4 serve to show that the surface states are sensitive to gas adsorption in a very specific way which we shall discuss in further detail below. These

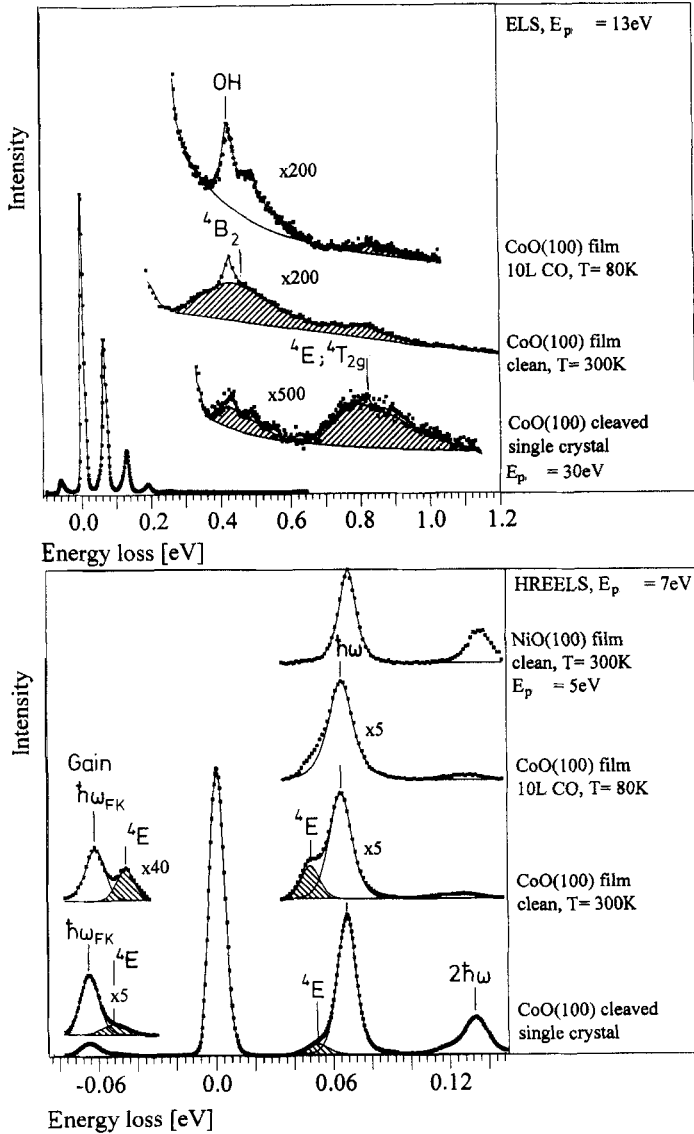


Fig. 5. Electron energy loss spectra of CoO(100). The lower panel shows the energy range of phonon losses and gains for a cleaved CoO(100) single crystal as well as a thin CoO(100) film. The upmost trace in the lower panel shows the behaviour of the losses upon CO adsorption. The upper panel shows the range of electronic losses for the cleaved crystal, the thin film and the CO covered thin film

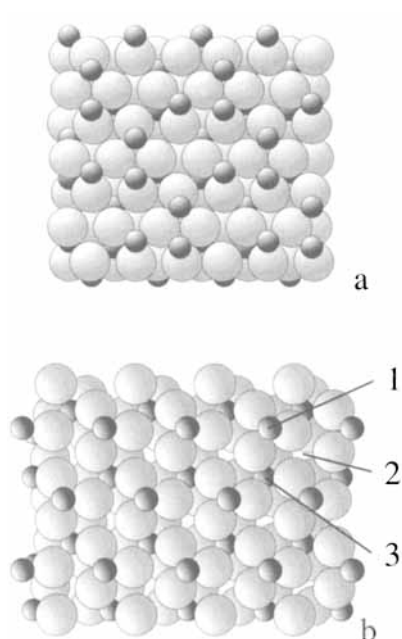


Fig. 6. a) Side view of the Cr_2O_3 structure perpendicular to the (111) direction. b) (111) surface of the Cr_2O_3 crystal cutting the buckled Cr^{3+} ion plane in two halves. The three possible sites 1, 2, and 3 for the Cr^{3+} ions are indicated

results for NiO are by no means unique. We have looked at the series NiO, CoO, and FeO [11]. A particularly interesting case is CoO [13]. Co in CoO is in a d^7 -configuration. This leads to low-lying excited states which are comparable to those found for NiO. However, there is one very low energy state for CoO(100) at 55 meV excitation energy which is actually situated in the region of phonon excitations. Fig. 5 shows the experimental data together with an assignment based on calculations by Staemmler and coworkers [13]. The feature at 55 meV (found in the loss spectrum as well as in the gain spectrum) is due to an excitation of the single electron between the two nondegenerate components of the former t_{2g} -orbital. The state at 0.45 eV corresponds to the surface state at 0.6 eV in the case of NiO, i.e. a transition between the former t_{2g} - and e_g -orbitals, split appropriately. In addition, Fig. 5 also shows the interaction of the surface with gases which we shall discuss in detail below. The two examples clearly demonstrate that ELS may be used to establish a surface ligand field spectroscopy to identify excited states localized in the surface. Those may be used in turn to investigate the interaction with adsorbed molecules. Such information is very hard to obtain for example with traditional XPS investigations because the metal core hole spectra of transition metal oxides are rather complicated and congested with many particle satellites [14, 15].

Only a few studies deal with the polar, nonstable surfaces. One example from our laboratory has been the water induced deconstruction of the octopolar reconstructed polar NiO(111) surface [8]. In this case the structural rearrangement involves three layers of the oxide. The mass transport involved leads to a relatively disordered surface indicated by diffuse LEED superstructure spots. There are other polar surfaces, however, where the creation of the most stable surface does not involve more than the top layer. For example, the (111) surface of Cr_2O_3 [16 to 20], (see Fig. 6a) may be created by cutting the crystal perpendicular to the (111) direction along a plane dividing the buckled plane of Cr^{3+} ions such that half of the Cr^{3+} ions remain on the surface. Fig. 6b shows the resulting surface structure. There are three possible positions for the Cr^{3+} ions on the surface (site 1, site 2, site 3), not all of which are occupied in a bulk terminated structure, and it is not at all clear that the position corresponding to the bulk structure is the most stable site for the Cr^{3+} ions on the surface. Via a simple site hopping mechanism involving nearest neighbour positions, one structure could be driven into the other one. We have investigated the Cr_2O_3 (111) surface structure via LEED [20].

The freshly prepared oxide surface was cleaned by flashing to 1000 K. While the sample was cooled down, its LEED structure (Fig. 7) was recorded with a conventional photo-

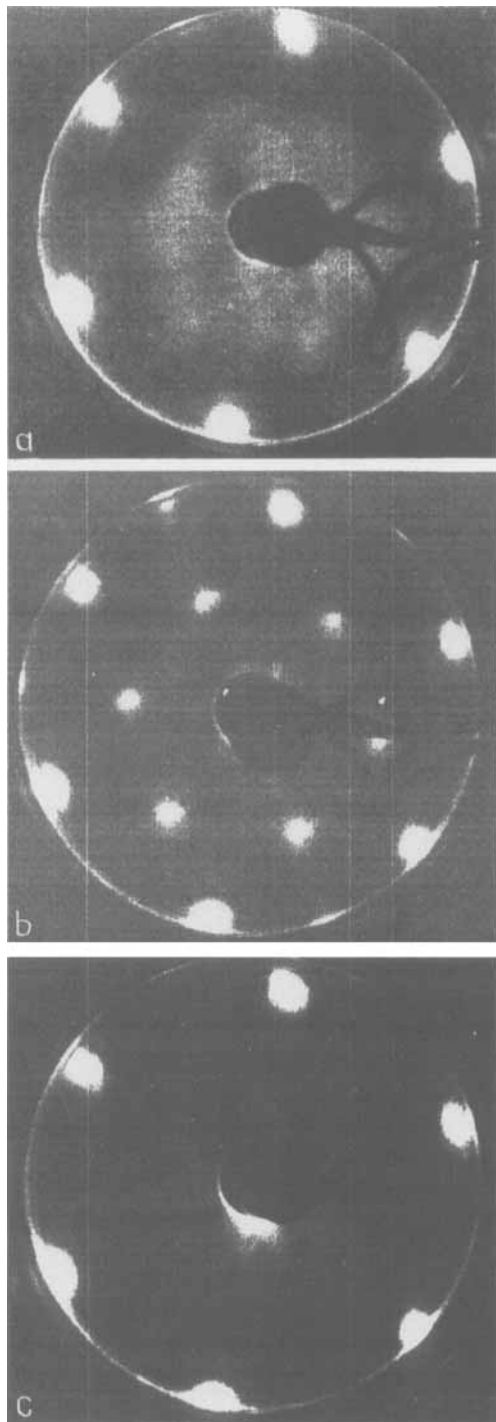


Fig. 7. LEED photographs (primary energy: (23.7 ± 0.1) eV) of the chromium oxide $\text{Cr}_2\text{O}_3(111)/\text{Cr}(110)$ surface after flash to 1000 K taken at different temperatures: a) ≈ 300 , b) ≈ 140 , c) ≈ 90 to 100 K

camera. At room temperature the main reflexes spanned a simple hexagon (Fig. 7a). Additionally, a hexagonal diffuse patch surrounding the (0, 0) reflex was observed. Upon cooling the diffuse intensity transformed into a $(\sqrt{3} \times \sqrt{3})R 30^\circ$ superstructure showing its maximum intensity at ≈ 140 K (Fig. 7b). Below this temperature the superstructure vanished again and finally a simple hexagonal LEED pattern without any additional structure at 90 K was recovered (Fig. 7c). The whole temperature dependence was reversible, i.e. it could be observed also when the sample was warmed up starting at 90 K.

Fig. 8 contains a plot of the intensity within an area indicated in the inset around the first order superstructure spot as a function of temperature. It is quite clear that the transition towards lower temperature leads to a complete attenuation of the superstructure spot, while the transition towards higher temperature only leads to a partial loss of intensity but an increased diffuseness of the superstructure. This is strong indication that we are dealing with an order-to-order transition at low temperature and an order-to-disorder transition towards higher temperature.

Also, the superstructure showed a pronounced sensitivity to adsorption of various molecular species. At its maximum intensity, i.e. at ≈ 140 K, the superstructure was exposed to $(6.65 \text{ to } 10.64) \times 10^{-6}$ Pa carbon dioxide which is known to strongly chemisorb on the chromium oxide surface [18]. The superstructure is quenched imme-

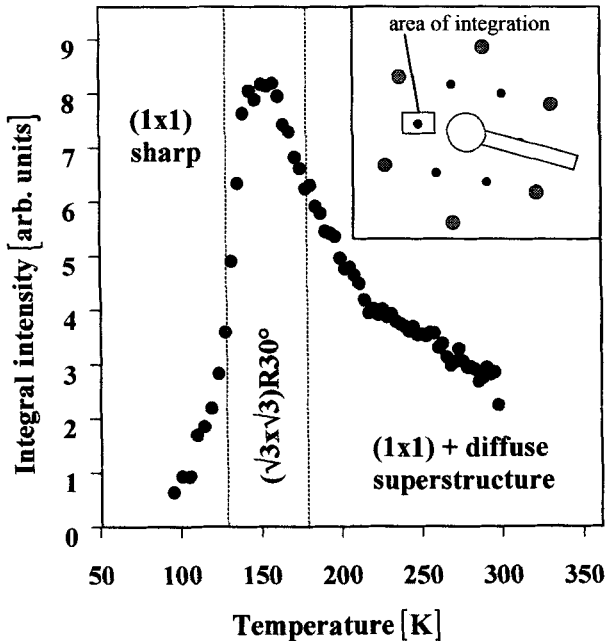


Fig. 8. Temperature dependence of the first-order superstructure spot intensity of the $(\sqrt{3} \times \sqrt{3})R 30^\circ$ superstructure. The inset indicates the area in reciprocal space used for intensity determination

diately after the onset of exposure. It could only be recovered by flashing the sample to that temperature at which thermal desorption of the corresponding species takes place, i.e. ≈ 400 K for carbon dioxide.

From the adsorption experiments we conclude that the structural rearrangement on the clean sample takes place directly at the surface and that the interaction between the adsorbates and the substrate strongly influences the energetics of the structural rearrangement at the surface. In order to gain further information on the local environment of the Cr^{3+} cations in the surface, we performed ELS measurements [20] similar to those described for NiO [12] and CoO [13]. Fig. 9 shows EEL spectra taken from the clean, flashed oxide surface at different temperatures. At 90 K the spectrum exhibits two signals at loss energies of ≈ 1.2 and ≈ 1.4 eV, denoted by A and B, respectively. They are accompanied by a broad feature C at about 1.8 eV. As the temperature rises, signals A and B lose relative intensity whereas the relative intensity of feature C increases. In order to assign the features to surface states, we have studied adsorption. Fig. 10 shows the EEL spectrum of the clean chromium oxide surface at 90 to 100 K as compared to spectra of the same surface after exposure to different gases [20, 21]. The spectrum in the considered energy region changes dramatically when various adsorbates are present. Thus we assign signals A through C to d-d transitions of surface chromium ions which are sensitive to the presence of adsorbates. Feature C, may also contain some intensity of d-d excitations of bulk chromium ions in a distorted octahedral crystal field. This assignment is supported by optical spectra of bulk chromium samples [22] as well as of ruby crystals [23] and is also in line with the observation that in the range of feature C some intensity remains after adsorbate formation. Parallel to the temperature dependence of the LEED data we also observe a temperature dependence of the ELS data as shown in Fig. 9, where we see a change of the intensity distribution for peaks A, B, and C. Let us assume for the moment that a Boltzmann ansatz is appropriate

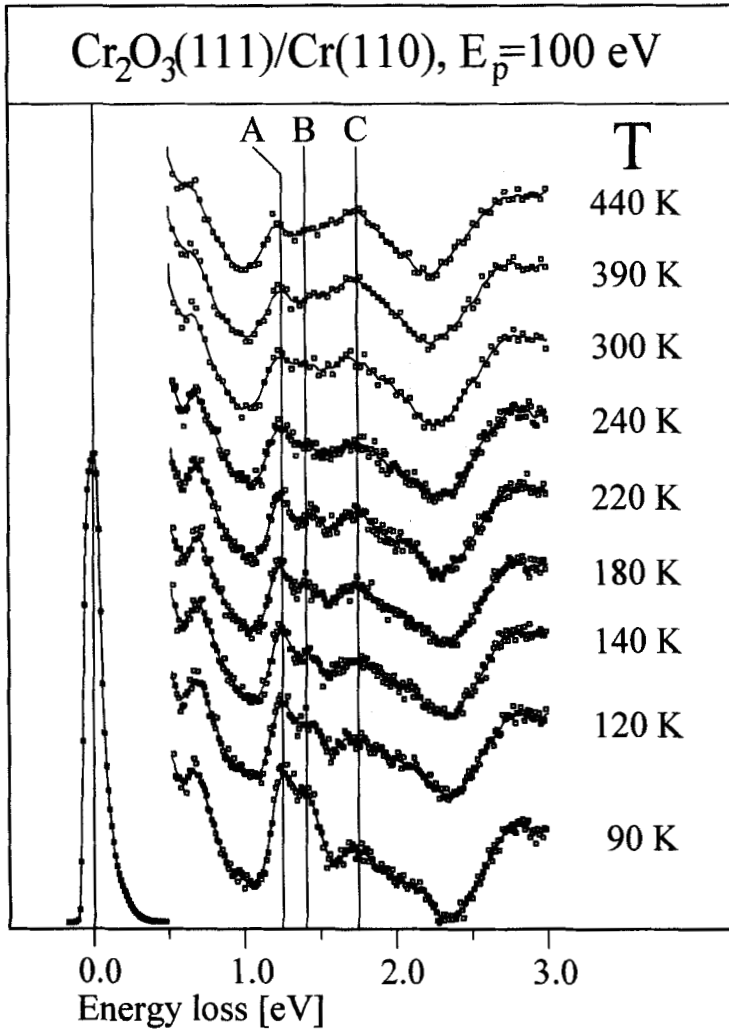


Fig. 9. Electron energy loss spectra of the clean flashed chromium oxide surface at different temperatures. The spectra were taken in specular detection at 100 eV primary energy of the incident electrons. The resolution was set to ≈ 150 meV as can be seen from the FWHM of the no-loss signal. The three signals mentioned in the text are denoted as A (≈ 1.2 eV), B (1.4 eV), and C (1.8 eV), respectively

to describe the processes (which could be debated), then we can plot the ratio of intensities of feature A and feature C versus $1/T$ which results in Fig. 11. From the shape we may deduce an energy difference of 8 meV between the state of the surface characterized by feature A and the state of surface characterized by feature C. This energy difference is of the order of magnetically dominated interactions.

This assignment is corroborated by quantum chemical ab-initio cluster calculations from the Staemmler group [20]. The cluster consists of one Cr^{3+} ion surrounded either by six O^{2-} ions which form a slightly distorted octahedron (bulk Cr_2O_3) or by three O^{2-} ions which represent the next neighbours of a Cr^{3+} ion at the (111) surface. This cluster is

embedded in an infinite or semiinfinite field of point charges $+3e$ and $-2e$ which simulate the Madelung field of the Cr_2O_3 ionic crystal. Within both the cluster and the point charge field the experimental crystal structure of bulk Cr_2O_3 [19] was used. Cr^{3+} is a d^3 -system, and its electronic ground state in the gas phase is a 4F state which is split in an octahedral crystal field into a $^4A_{2g}$ ground state, a first excited $^4T_{2g}$, and a second excited $^4T_{1g}$ state. The threefold spatial degeneracies of the excited states of T_{2g} and T_{1g} symmetry are further split (by about 0.02 eV) in the slightly distorted octahedral crystal field of bulk Cr_2O_3 . The lowest excitation energies are calculated at the CASSCF (complete active space self-consistent field) level to be 1.73 eV ($^4T_{2g}$) and 2.73 eV ($^4T_{1g}$) which compares quite favourably with the EELS data of 2.0 and 2.8 eV [20].

At the $\text{Cr}_2\text{O}_3(111)$ surface the Cr^{3+} ions are exposed to a weaker crystal field since half of the oxygen ions are removed. Furthermore, this field has only (distorted) C_{3v} symmetry as compared to the higher O_h symmetry in bulk Cr_2O_3 . Therefore, one can expect that the

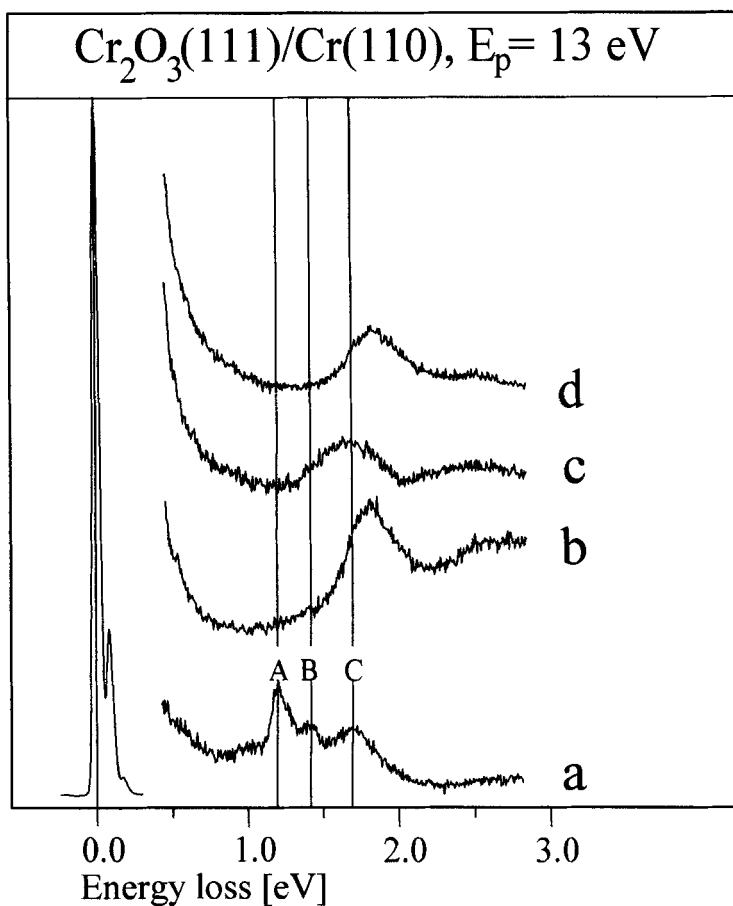


Fig. 10. Electron energy loss spectra of the chromium oxide $\text{Cr}_2\text{O}_3(111)/\text{Cr}(110)$ surface after flash to ≈ 1000 K and cooling to 90 K; (a) without adsorbate, (b) after adsorption of CO, (c) after adsorption of NO, (d) after adsorption of CO_2

energy differences between the components of 4F are smaller at the surface than in the bulk and that the quasidegeneracies of the T_{2g} and the T_{1g} levels are split. Fig. 12 shows our CASSCF results for the three nonequivalent Cr^{3+} ions at the $Cr_2O_3(111)$ surface (sites 1, 2, 3, Fig. 6) and confirms this expectation: For all three positions both the ${}^4T_{2g}$ and the ${}^4T_{1g}$ states are lowered considerably relative to the ${}^4A_{2g}$ ground state and are slightly split (${}^4T_{2g}$ into 4A_1) and 4E ; ${}^4T_{1g}$ into 4A_2 and 4E). Despite of these similarities, the d-d spectra of the Cr^{3+} ions at the three nonequivalent sites differ to some extent. Due to the weaker ligand fields, the Cr^{3+} ions at the sites 2 and 3 have considerably smaller excitation energies (the lowest ones at about 0.9 and 1.5 eV) than those at site 1 (1.05 and 1.26 eV). If we assume that the calculated excitation energies of the components of ${}^4T_{2g}$ are by 0.1 to 0.2 eV too low, the d-d excitation energies for the Cr^{3+} at site 1 are in reasonable agreement with the measured EELS spectra, while those of the Cr^{3+} ions at sites 2 and 3 are considerably lower.

In these calculations the Cr^{3+} ions have been given fixed positions. For the two sites, occupied in the bulk, the choice could be based on those interatomic distances known from the bulk, for the third position, which is not occupied in the bulk, a reasonable position has been assumed. If one allows for geometry relaxation one observes a very interesting effect: the Cr^{3+} ion residing in site 1 exhibits a stable geometry with internuclear distances very near the bulk values. Its equilibrium position is moved slightly (by 0.15 Å) towards

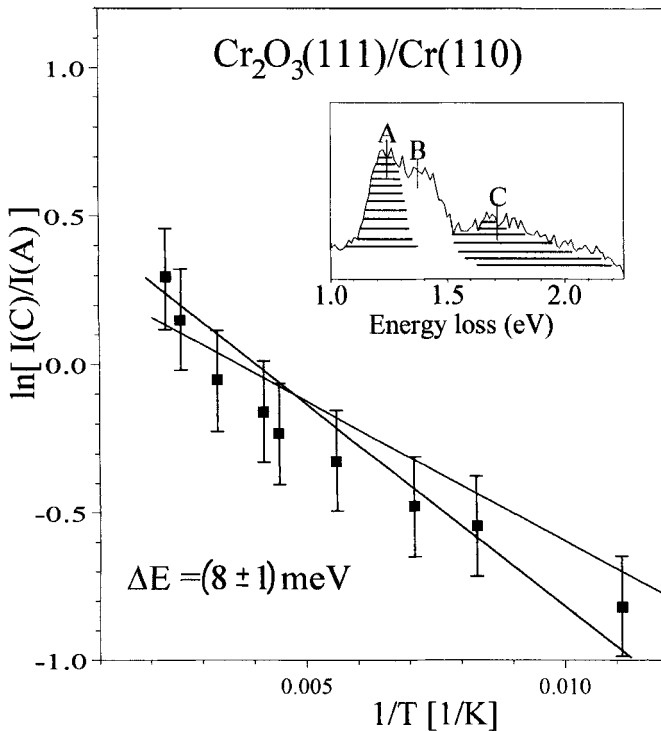


Fig. 11. Temperature dependence of the chromium oxide $Cr_2O_3(111)/Cr(110)$ surface states as analyzed from Fig. 9. The inset shows the areas under peaks A and C, respectively, which have been taken into account for the data analysis

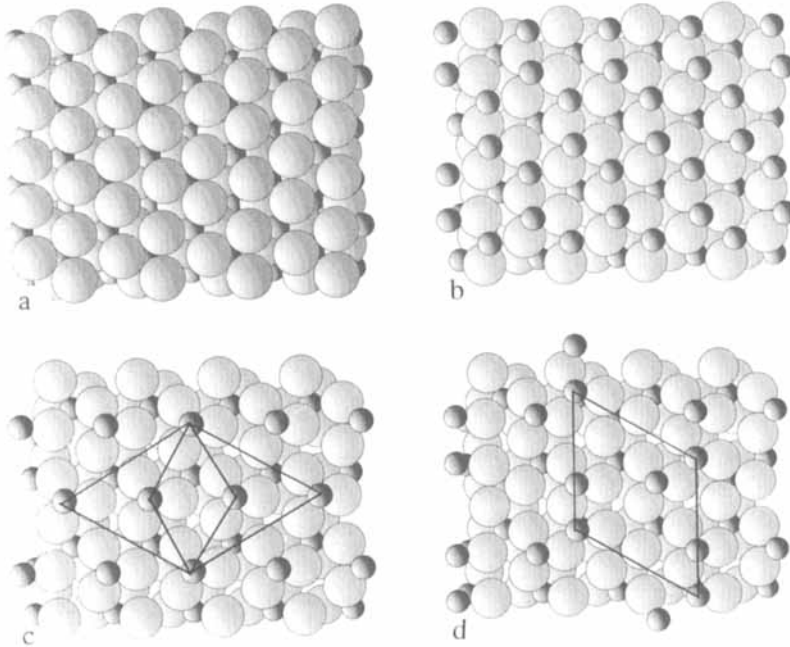


Fig. 13. Three different terminations of the chromium oxide surface: a) by a close oxygen atom layer, b) by a full chromium ion layer, c) by half a chromium ion layer, unit meshes (1×1) and $(\sqrt{3} \times \sqrt{3}) R 30^\circ$ are shown, d) possible chromium ion arrangement leading to a $(\sqrt{3} \times \sqrt{3}) R 30^\circ$ mesh

In the following we will propose a model which explains the structural changes on the clean chromium oxide surface. We will start with a model for the system at 90 to 100 K and then consider mechanisms possibly involved in the phase transition.

Fig. 13a to d show truncations of the bulk α -corundum-type chromium oxide crystal structure [24] parallel to the (111) plane with three different possible terminations. Fig. 13a shows the termination by oxygen ions, Fig. 13b the termination by a complete, buckled chromium ion layer. In both cases the surface is electrostatically unstable. However, if only half of the Cr^{3+} ions remain on the surface, the resulting charge density on the surface is reduced to half of its value in Fig. 13b. This surface is electrostatically stable [4]. We propose Fig. 13c as a possible model for the simple (1×1) surface structure found in LEED at 90 to 100 K (Fig. 7c). Upon rising the temperature above 100 K, a $(\sqrt{3} \times \sqrt{3}) R 30^\circ$ structure appears indicating a larger unit cell. The low transition temperature of 140 K already provides evidence that the process is connected with a relatively low activation energy. As a rule of thumb one would estimate activation energies in the range of 0.3 eV which would be consistent with surface diffusion processes. The kind of structure resulting from such diffusion processes is indicated in Fig. 13d. There are several reasons why such a structural rearrangement may take place:

Starting with the situation at lowest temperature we believe that the Cr^{3+} ions are all in equivalent sites. These sites could be those also occupied in the bulk (site 1, Fig. 6). There are two more threefold sites (sites 2 and 3, Fig. 6) which are available for occupation. One of course, is the other site occupied in the bulk (site 2). It is characteristic of this site that there is never a Cr^{3+} ion in the second layer below the top oxygen layer. The second

alternative is the site characterized by an open oxygen triangle (site 3). There are Cr^{3+} ions in the second layer below this site. The question is, which is the most stable site populated at lowest temperature. Our ELS data in comparison with the theoretical calculations indicate that the outer Cr^{3+} sites (site 1) are occupied at lowest temperature. Each surface Cr^{3+} ion has a direct counterpart in the next layer down. If we assume a magnetic coupling in the first layers similar to the bulk situation, then there is antiferromagnetic coupling to the second Cr layer down of the order of 12 meV [25], but within the topmost layer the Cr ions are ferromagnetically or very weakly antiferromagnetically coupled. The magnetic coupling that is important in this case, is between the topmost Cr^{3+} layer and the one below the quasi-hexagonally packed O^{2-} layer. Locally, this means that two Cr^{3+} ions are exchange-coupled via three oxygen ions forming a $\text{Cr}^{3+}-\text{O}-\text{Cr}^{3+}$ angle of approximately 85° . This situation is similar to a dinuclear Cr^{3+} complex where the transition metal ions are bridged by three hydroxyl groups. In this latter case the exchange splitting has been measured to be 8 meV [26]. This energy has to be surmounted to magnetically decouple the ions. If the temperature is raised, half or less of the Cr^{3+} ions at the surface may be decoupled from the second layer and may change site. Consequently, a larger unit cell with a $(\sqrt{3} \times \sqrt{3}) R 30^\circ$ unit mesh is observed. A schematic representation is shown in Fig. 13d. As is revealed by the schematic drawing the Cr^{3+} ions reside only in sites that have a second Cr^{3+} ion underneath in the second layer. There are basically two reasons for this. Primarily, the thermal dependence of the EEL spectra is consistent with this occupation. The intensity of the surface peaks A and B goes down indicating that the occupation of site 1 is reduced. Since site 2 is not stable with respect to the motion of the Cr^{3+} through the oxygen plane into the second layer, the Cr^{3+} ions can only move to the stable site 3. Secondly, there is an antiferromagnetic coupling among the Cr^{3+} ions in each Cr layer, which is about half as large as through the $\text{Cr}-\text{O}_3-\text{Cr}$ bridge [26]. Therefore, each ion is antiferromagnetically coupled within the top layer and also with respect to the second Cr^{3+} ion layer down. Such effects may represent the driving force for the process to occur. The energy differences between differently magnetically coupled states are of the order of 6 meV [26] compatible with our temperature dependent EEL spectra.

At higher temperature the two different Cr^{3+} sites at the surface are statistically occupied, giving rise to a unit mesh typical for a lattice gas. This again leads to a $p(1 \times 1)$ structure with very diffuse intensity in the range of the $(\sqrt{3} \times \sqrt{3}) R 30^\circ$ positions. This sequence of events would explain the observed changes of the diffraction patterns as well as the changes of the EL spectra. The latter will be considered in more detail in the following: The key aspect is the exchange between the two inequivalent Cr^{3+} sites on the $\text{Cr}_2\text{O}_3(111)$ surface. We have shown that the inequivalent ligand fields for the two sites lead to different d-d excitation energies. Therefore the d-d transitions in the EL spectra may be used to follow the site exchange process. Fig. 9 shows at lowest temperature a d-d spectrum which is compatible with the spectrum calculated for the Cr^{3+} ion site 1. We assume that the magnetic exchange with the second layer favours this geometry. Upon heating the surface we propose that site 3 becomes populated. This is documented by a redistribution of intensity in the sense that the peak at 1.4 eV is washed out at the expense of the feature at 1.75 eV which appears to become broader. Comparing with the calculated energies we see that the ${}^4\text{E}$ and ${}^4\text{A}_1$ states at lowest excitation energies are close in energy which contribute to the leading peak but take intensity out of the second peak. The two ${}^4\text{A}_2$ and ${}^4\text{E}$ states at higher energies are, however, lower than the corresponding excitations for the "outer" Cr^{3+} ions thus leading to an increase of width of feature C. It is thus clear that the changes observed

in the EL spectra are fully compatible with the proposed changes in the LEED patterns. Also, the observed order-order transition behaviour towards low temperature, and the order-disorder transition behaviour towards higher temperature is fully in line with the observation.

4. Molecular Adsorption on Oxide Surfaces

Contrary to metal surfaces, where bonding is strong ($\Delta E_a \approx 1$ to 2 eV) due to σ/π charge exchange between the molecule and the surface [27] bonding to a (100) oxide surface of rock-salt type is dominated by multipolar electrostatic forces, which leads to rather weak bonding ($\Delta E_a \approx 0.1$ to 0.5 eV). As a consequence of the rather weak bonding, energy

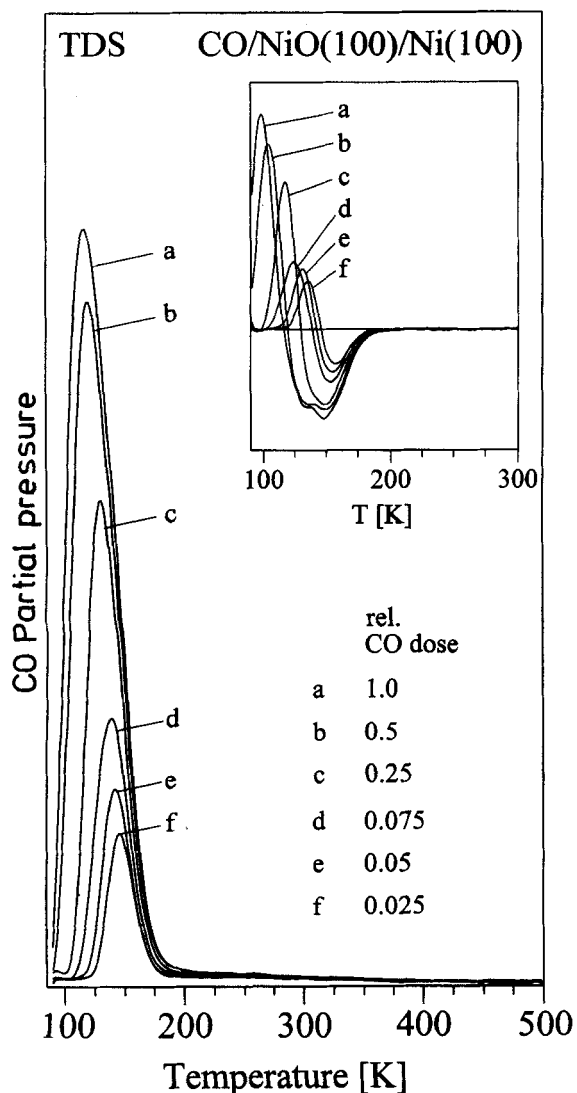


Fig. 14. Thermal desorption spectra of the system CO/NiO(100) as a function of CO coverage. The inset shows the first derivatives of the spectra

differences between various orientations of molecules, i.e. bonding of CO with its C end versus O end towards the surface or parallel to the surface are rather small and of the order of 0.05 to 0.1 eV [28 to 30]. Since these energy values are well within the error range of the theoretical predictions, experimental studies are needed.

Fig. 14 shows the TD spectra of CO/NiO(100) [31] taken as a function of coverage. It is clear from the spectra that the maxima of the desorption features only exhibit a very slight variation with CO coverage. The situation becomes more evident by looking at the first derivatives of the TD spectra as shown in the inset of Fig. 14. At low coverage there is a single peak contributing to the spectra while at higher coverage (dose >0.12) a slightly shifted second peak fills in. We have analyzed the spectra according to a simple Redhead procedure [32a] assuming a prefactor of 10^{13} , which is the standard value [32b]. Depending on coverage this yields a value of 29.3 to 36.8 kJ mol⁻¹ for the adsorption enthalpy. This may be compared with a value of 38.5 to 52.3 kJ mol⁻¹ recently published by Vesecky et al. [33] on the basis of isosteric measurements using IRAS. The vibrational frequencies determined in the present study on the basis of ELS measurements are not very precise but in line with the values reported by Vesecky et al. [33] for the CO stretching modes.

The adsorption energies of CO/NiO(100) may be compared with those determined for NO/NiO(100) [34]. The latter system is slightly more strongly bound, i.e. by 51.0 kJ mol⁻¹ as determined by the same Redhead procedure [31] and based on TD- spectra. This higher adsorption energy reflects the different bonding characteristics for CO and NO as predicted by theoretical calculations performed in several groups [28 to 30, 35 to 39] but for the CO/NO comparison in detail by Staemmler and his group [28, 35]. While CO is held almost exclusively by multipolar electrostatic interactions, NO bonding to NiO(100) does exhibit some covalent chemical bonding characteristics. This is due to the additional unpaired electron on NO as compared to CO as has been discussed in [14]. This discussion indicated, and was verified experimentally, that the NO/NiO(100) bond leads to a tilted geometry with the ON–Ni bond angle in the neighbourhood of 135°. However, for the CO/NiO(100) bond equivalent calculations predict a linear geometry with a Ni–CO angle of 180°.

We have investigated the orientation of CO on NiO(100) via NEXAFS (near edge X-ray absorption fine structure) [31]. The result is a perpendicular orientation. NO, on the other hand, exhibits a 45° tilt with respect to the surface normal for the same substrate.

However, with the NEXAFS analysis it is not possible to decide whether the CO molecule for example, is oriented with the carbon end or with the oxygen end towards the surface. While for typical strong CO–transition metal bonds there is no question that the molecule binds to the surface via the carbon atom (exceptions are very rare) [27] in the case of oxide surfaces where bonding is much weaker, the binding energies of the two orientations differ only by less than 0.05 to 0.1 eV [28 to 30, 35 to 39]. One way to tackle this question is valence photoelectron spectroscopy. The idea is simple and has been applied many times in the past [27]: The three outer valence ionizations of CO originate from the ionization of the carbon lone pair (5σ), the Co π bond (1π), and the oxygen lone pair (4σ). If the carbon atom is involved in the interaction, the 5σ orbital will be shifted relative to the other ionizations. Fig. 15 shows He II (unpolarized) angle resolved photoelectron (ARUPS) spectra taken at different angles of light incidence and different electron collection angles. These data serve two purposes: They are used to support the orientation determination via NEXAFS as well as to evaluate the bonding mechanism. Fig. 15a shows the raw data with and without CO coverage. Fig. 15b shows the difference spectra within the energy range of the CO induced features. In order to analyze these data, several points have to

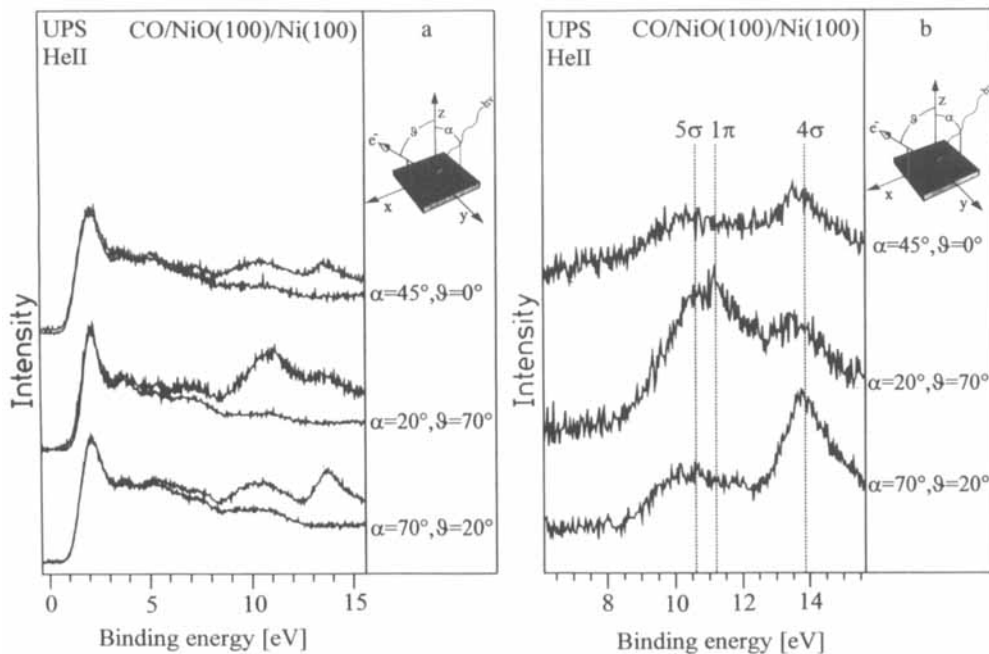


Fig. 15. a) Angle resolved photoelectron spectra of CO/NiO(100) in comparison with the clean substrates for different light incidence angles and direction of electron detection. b) Difference spectra between CO covered and uncovered substrates shown in Fig. 15a

be noted. Firstly, at He II photon energies the cross sections of the 4σ ionization is larger than the one of the 5σ ionization [40]. Secondly, the σ intensities peak if the light is polarized along the molecular axis and the electrons are collected near the direction of the oriented axis. Therefore, if the CO axis is oriented perpendicular to the surface, the choice of near grazing light incidence and normal detection would lead to maximal σ intensities [41, 42]. Strictly speaking, the analysis is simple only for fully linearly polarized light. In the present case, however, we have to consider unpolarized light [42]. In other words, there is always the possibility to ionize π states. We can only hope to vary the relative magnitude of π and σ ionizations in the following simplified manner if the axis is oriented normal to the surface: For grazing incidence and near normal emission we expect large σ intensities. For near normal incidence and grazing emission we expect dominance of π ionization. For 45° light incidence and normal emission the σ ionizations should dominate.

With this in mind we can analyze the spectra in Fig. 15 and find that they are consistent with an orientation of the molecular axis normal to the surface if we place the ionization potentials for the adsorbed molecule as indicated in Fig. 15b. We have collected the values from the present study as measured relative to the Fermi level in Table 1 [31], where we compare them to ionization energies from other CO adsorbate systems. Included are chemisorbeds on metal surfaces [43, 44] as well as a physisorbed system also on a metal surface [45]. The physisorbed layer behaves similar to a condensed CO layer [46] with relative ionization potentials almost identical to the gas phase [40] and only slightly shifted with respect to the absolute values of gas phase CO if referred to the vacuum level [27]: In the chemisorbed layer, on the other hand, two effects shift the relative and absolute

Table 1
CO binding energies of valence levels (in eV)

	5 σ	1 π	4 σ	ref.
Ni(100) c(2 \times 2)	8.1	7.5	11.1	[43]
Pd(111) c(4 \times 2)	8.2	7.3	11.0	[44]
Al(111)	8.2	11.1	13.8	[45]
NiO(100)	10.6	11.1	13.9	[31]

ionization potentials. The strong CO–metal bond via the carbon atom leads to the pronounced shift of the 5 σ ionization to a value below the 1 π ionization energy. In addition, hole state relaxation in the final ion state due to the screening by the metal electrons shifts the complete spectrum to considerably lower ionization energies giving rise to the strong deviations from the values observed for the physisorbed system [27]. This is well known in the literature [27] and has been repeated briefly here in order to judge the values observed for the oxide surface properly. The analysis is now very easy. 1 π and 4 σ ionizations are slightly shifted with respect to the values of the physisorbed system indicating similar CO–substrate interaction strengths. However, the carbon lone pair (5 σ) is shifted more strongly than the 1 π and 4 σ ionizations indicating a preferential interaction of the molecules through the carbon end. Hole state screening is of similar magnitude as in the physisorbate which is reasonable, given that the oxide surface should be less polarizable as compared with a metal.

Therefore, the present analysis of the ARUPS data indicates that the molecule is bound to the surface via the carbon end in an upright position and with relatively low adsorption energy. Thus, the present experimental results are in full agreement with the above mentioned theoretical predictions [28 to 30, 35 to 39].

So far we have not explicitly determined the adsorbate site. This can be done via a study of the oxide surface states because they are due to excitations strongly localized on the Ni sites. If a molecule is bound to this site, then the d–d excitation will shift. Fig. 4 exhibits this effect when NO is dosed a NiO(100) surface [12]. The same is found for CO exposure. However, OH adsorption through water dissociation does not happen at this site, because the OH vibrations (as shown in Fig. 7) are clearly visible but the surface state is not shifted, indicating that water dissociation occurs at defect sites. We have shown elsewhere that the study of polar surfaces of rock-salt structured materials gives us some hints that this is the case [10, 11, 47].

A polar surface that lends itself to detailed investigations, is the Cr₂O₃(111) surface discussed above. One reason is that it can easily be prepared OH-free in contrast to the polar surfaces of the rock-salt type oxides [10, 11, 47].

A relatively detailed picture of the adsorption behaviour has been established for CO adsorption. Fig. 16 shows photoelectron spectra of the ($\sqrt{3} \times \sqrt{3}$) R 30° CO structure [16] recorded as a function of detection angle. In particular Fig. 16 shows a set of photoelectron spectra taken with a constant angle, i.e. 90°, between the directions of light incidence and electron detection.

From Fig. 16 it is obvious that the σ ion states exhibit highest intensities for near normal light incidence and near grazing electron emission whereas at grazing light incidence these features are strongly attenuated, in strong contrast to CO adsorbed standing up on most

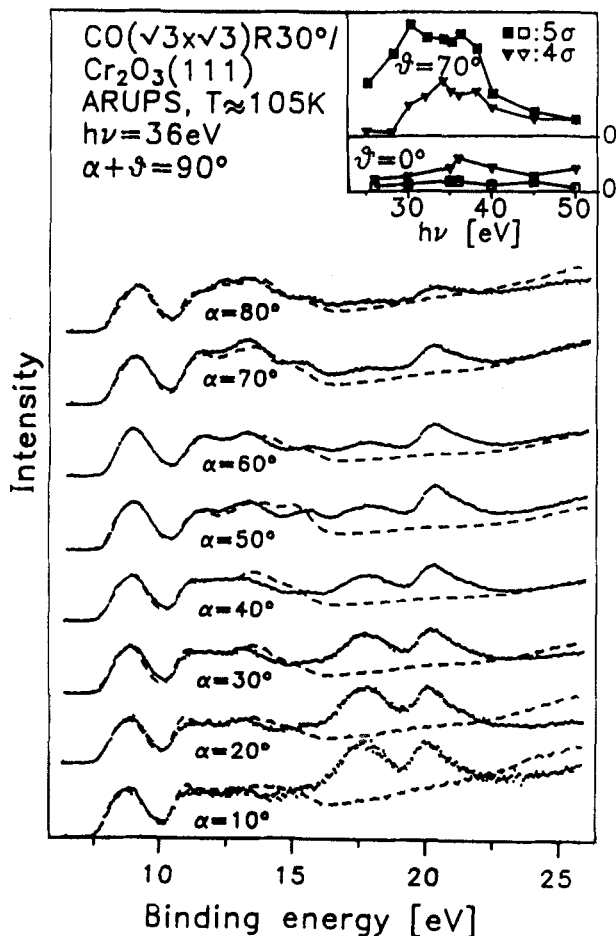


Fig. 16. Photoelectron spectra at various detection geometries. The inset shows the variation of the peak intensities with photon energy

metal surfaces. Since at a photon energy of 36 eV the σ states emit with highest intensity if the polarization direction and the direction of electron detection both coincide with the CO molecular axis, this behaviour is only compatible with an orientation of the molecular axis approximately parallel to the surface. In the inset of Fig. 16 we compare the emission intensities of the CO σ valence states as a function of photon energy for two different experimental geometries. The data shown in the upper panel were taken at a light incidence angle of 20° with respect to the surface normal, collecting the electrons 70° off normal whereas the data in the lower panel were taken at normal electron emission and near grazing light incidence ($\alpha = 80^\circ$). Obviously a strong σ -shape resonance is observed only for grazing electron detection, again clearly indicating that the CO molecules must be strongly tilted. NEXAFS data show that the intensity of the π resonance varies only slightly as a function of the light incidence angle as expected for CO molecules lying flat on the surface since one 2π component is oriented parallel to the surface whereas the other one sticks out of the surface. A quantitative estimation of the tilting angle was not possible from our NEXAFS data since the σ resonance was so weak that its intensity only could be evaluated with very large error bars.

From the data discussed so far a quantitative evaluation of the tilting angle was not possible, but it could be estimated to be larger than 70° . An open question still is: where do we locate the 1π ionization? For flat lying CO molecules the 1π levels are expected to split into two components, $1\pi_{xy}$ and $1\pi_z$, the first one oriented parallel to the surface and the other one oriented perpendicular to the surface. Whereas the $1\pi_{xy}$ emission might be hidden below the σ emissions because this level should be intense at grazing emission angles like the σ orbitals, the $1\pi_z$ should be intense at normal emission where the σ emission is weak. As can be seen from Fig. 16 the 5σ emission is nearly totally suppressed at near normal electron emission so that the $1\pi_z$ level is most likely not situated near to the 5σ level as is the case for the 1π levels of CO adsorbed on most metals. One might suppose that the $1\pi_z$ level is located somewhere in the region of the substrate bands but since the $1\pi_z$ orbital will interact strongly with these bands it will most likely be shifted to higher binding energy because the substrate levels are energetically located above the 1π levels. Considering this it seems to be rather unlikely that the 1π levels are located somewhere in the region of the oxide emission.

Whereas the 5σ emission is nearly totally suppressed at near normal emission a broad feature remains in the region of the 4σ between 19 and 22 eV (Fig. 16). Since the 4σ and the 5σ emission intensities should behave similar, it is tempting to attribute the remaining emission between 19 and 22 eV to the $1\pi_z$ level. Another possible assignment would be that this feature is due to a σ shake-up state. However, we consider this to be unlikely because such shake-up states should be intense at emission angles where the σ main lines are also intense, which is not the case.

Fig. 17 compares the spectra of CO on NiO and Cr_2O_3 with data reported in the literature for free condensed CO as well as CO adsorbed on metal surfaces covering a wide range of adsorption energies [27, 48]. All binding energies for the oxide systems are larger than the corresponding values known from metal surfaces. The most interesting finding, however, is the energetic position of the $1\pi_z$ level which is in the present case most likely situated near to the 4σ level, indicating a fundamentally different interaction of the molecule with the surface as compared with all cases observed so far: The CO lone pairs (4σ and 5σ) we propose to be bound towards two different Cr ions in the sense of two σ donor bonds which shift the σ binding energies to higher values. If this is true then it is very reasonable to assume that the 1π levels interact with both the Cr ions, but in addition, and more importantly, with the oxygen layer underneath the terminating Cr layer. This latter interaction between the closed shell O^{2-} ions and CO must be basically repulsive. Since the oxygen levels are situated at lower binding energies than the CO 1π levels, the $1\pi_z$, which is the one that strongly interacts with the O^{2-} ions, is shifted towards higher binding energy and the interacting O^{2-} levels are rearranged as well. The shift of the $1\pi_z$ level is recognized in the data, while it is more difficult to identify the effect onto the oxygen levels. If we judge the observed shifts of CO on $\text{Cr}_2\text{O}_3(111)$ with respect to gaseous CO we find a shift of all CO levels to higher binding energies. The shift of the 5σ level is larger than the one of the 4σ level. This is very reasonable because it follows the individual polarizabilities of the levels involved. The interaction may be separated into the two bonding Cr-CO(5σ) and Cr-OC(4σ) interactions, and into a repulsive O^{2-} -CO(1π) interaction, leading to a weakly chemisorptive CO- Cr_2O_3 bond.

A definite structure model of CO on the Cr-terminated patches of $\text{Cr}_2\text{O}_3(111)$ cannot be presented at present but we find a $(\sqrt{3} \times \sqrt{3})\text{R } 30^\circ$ superstructure in LEED. The LEED pattern is extremely electron beam sensitive.

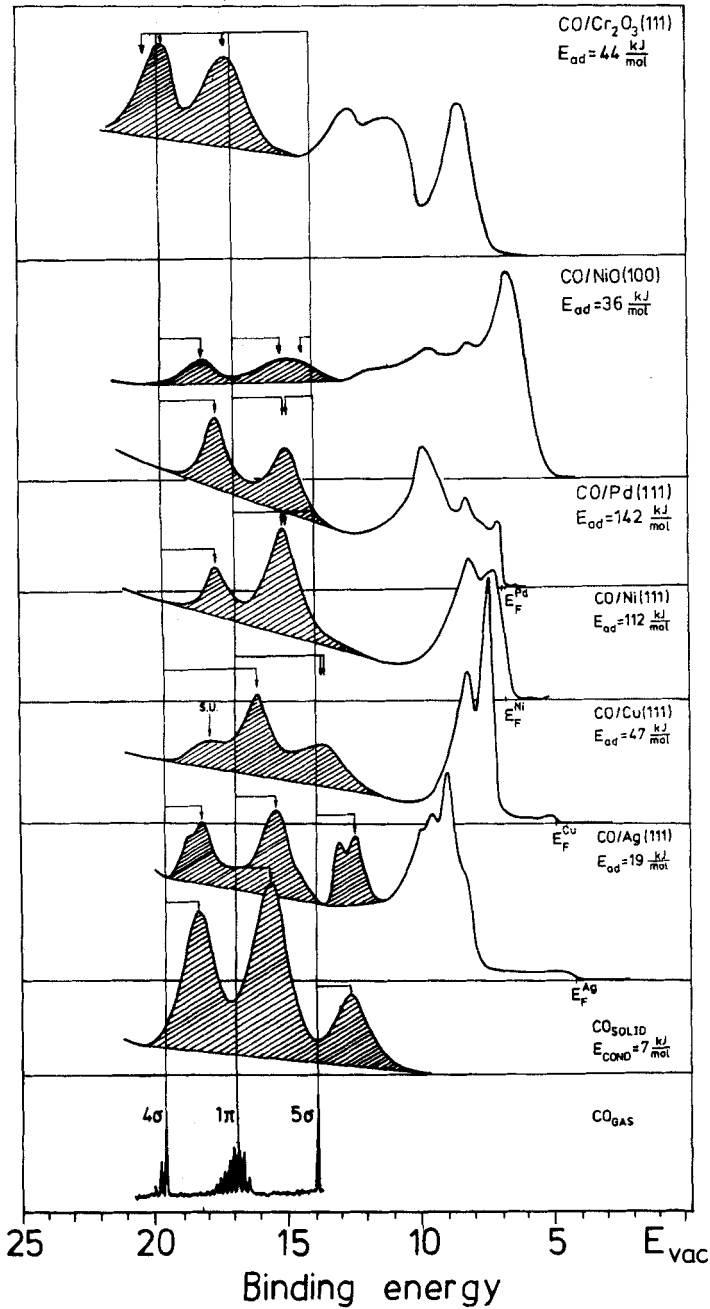


Fig. 17. Photoelectron spectra of CO adsorbed on metal and metaloxide surfaces in comparison with gas phase and condensed CO. The spectra are taken in normal electron emission. (S.U. means shake up)

5. Modification of Oxide Surfaces by Metal Deposits

Some of the most frequently studied metallic modifiers are alkali metals [49]. The reason is that alkali as well as alkaline earths act as electronic promoters in catalytic reactions. The influence of alkali on oxide surfaces is widely unexplored [19, 20, 50]. Therefore, we present in the following a brief overview of some of our results for sodium modification of

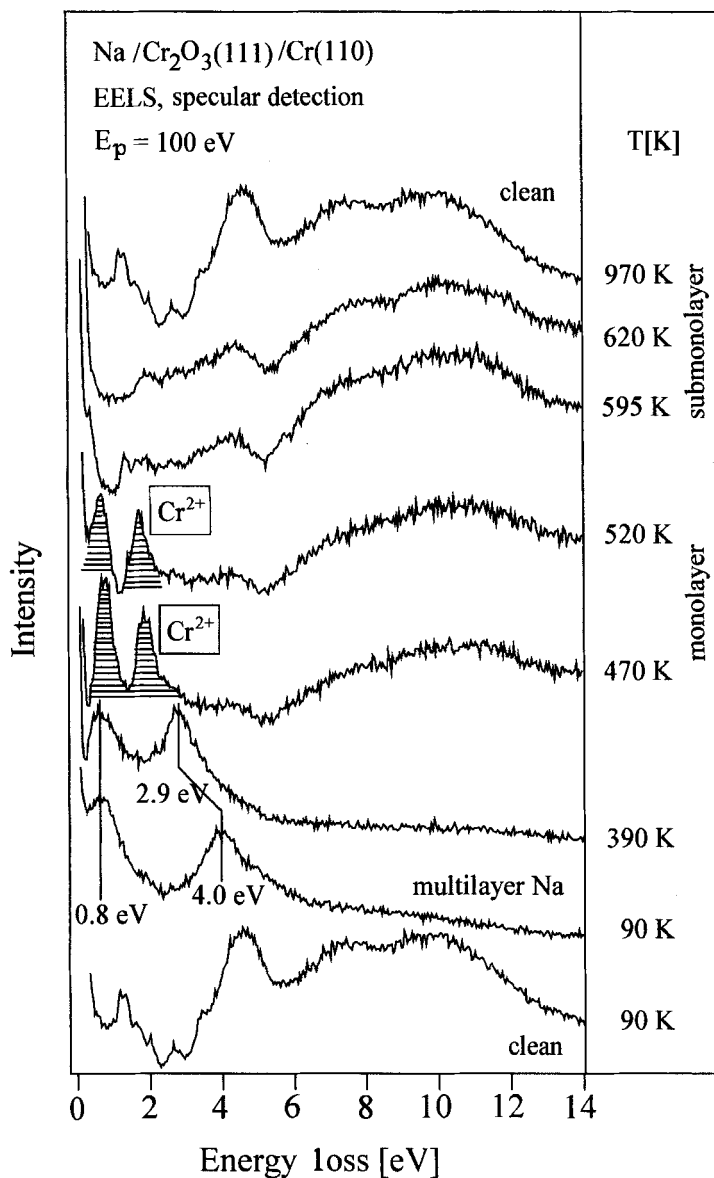


Fig. 18. Electron energy loss spectra of the clean and Na covered Cr₂O₃(111) surface. The surface was dosed with Na at 90 K to form a thick layer which was subsequently heated to the temperatures given. At 420 K Na monolayer coverage is reached. At 1000 K the surface is Na free

$\text{Cr}_2\text{O}_3(111)$ [19, 20, 51] and $\text{NiO}(111)$ [50]. I have chosen these two examples because the observed behaviour covers different situations to be encountered on an oxide surface. The idea is that while Ni is an ion that prefers a single oxidation state, i.e. 2+, Cr ions easily assume various oxidation states.

Fig. 18 shows the result of an ELS experiment [51], where a spectrum of the clean $\text{Cr}_2\text{O}_3(111)$ plane is shown as the bottom trace. We have discussed the assignment of the various peaks previously [16 to 20]. If a thick (several ML) layer of Na is deposited on the $\text{Cr}_2\text{O}_3(111)$ surface at 90 K, the substrate excitations disappear and two new bands are observed. As will be discussed in detail elsewhere [51], the band at 4.0 eV is due to the Na surface plasmon [52], the peak at 0.8 eV is assigned to a Na/oxide interface excitation [51]. Upon raising the surface temperature, some Na evaporates and the layer thickness is reduced, but it is still considerably larger than a monolayer. As is expected for thin metal films in contact with a dielectric on one side and vacuum on the other, the two interface excitations are coupled and they change energy as the thickness varies [53]. The Na surface plasmon changes the energy considerably from 4.0 to 2.9 eV while the interface ($\text{Cr}_2\text{O}_3(111)/\text{Na}$) only slightly varies from 0.8 to 0.7 eV. If the temperature is increased above 420 K the Na multilayer has completely been desorbed and we reach the monolayer regime. The spectrum taken at 470 K is characteristic of this situation. Substrate excitations between 6 and 14 eV are visible. However, in the d-d excitation regime below 3.5 eV we find new

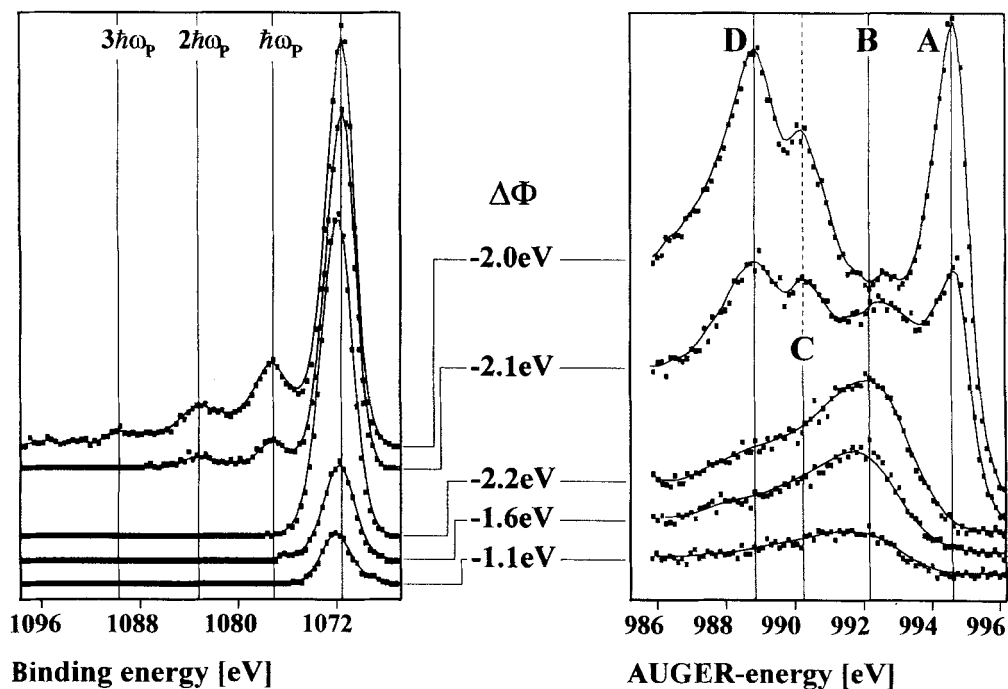


Fig. 19. Na 1s XPS spectra (left panel) and Auger Na KLL spectra (right panel) of the system Na/NiO(111) at different Na coverages as given by the value of the work-function change ($\Delta\Phi$). The work function changes almost linearly to -2.2 eV, passes through a minimum and reaches a saturation value (close to the one of bulk metal) at -2 eV

Table 2
Reaction enthalpies

$6 \text{ Na} + \text{Cr}_2\text{O}_3 \rightarrow 3 \text{ Na}_2\text{O} + 2 \text{ Cr}$	$\Delta_{\text{R}}H(300 \text{ K}): -104 \text{ kJ mol}^{-1}$
$2 \text{ Na} + \text{NiO} \rightarrow \text{Na}_2\text{O} + \text{Ni}$	$\Delta_{\text{R}}H(300 \text{ K}): -176.5 \text{ kJ mol}^{-1}$
$3 \text{ Mg} + \text{Cr}_2\text{O}_3 \rightarrow 3 \text{ MgO} + 2 \text{ Cr}$	$\Delta_{\text{R}}H(300 \text{ K}): -660 \text{ kJ mol}^{-1}$

sharp features. Ab-initio calculations by Staemmler [54] have shown that a Cr^{2+} ion in a threefold site at a $\text{Cr}_2\text{O}_3(111)$ surface has d–d excitations at exactly these energies. This allows us to propose that in the range of Na monolayer coverage the $\text{Cr}_2\text{O}_3(111)$ surface is covered with a Cr^{2+} layer. With decreasing Na coverage parallel to increasing surface temperature, the Cr^{2+} d–d excitations reappear, and finally close to 1000 K the surface is Na free and the spectrum of the clean surface is revealed. Interestingly, Na cannot reduce the Cr ions to the metallic state. However, if we switch from Na to Mg then we find metallic chromium on the surface [55].

On the other hand, Na reduces NiO to metallic Ni when the Na coverage increases above a certain coverage, as we shall discuss in the following.

At low temperatures we can grow an alkali monolayer which is associated with the observation of a work-function minimum. Upon increasing the layer thickness we eventually form a metallic overlayer. For Na on NiO(111) we show in Fig. 19 a series of XP and Auger spectra for increasing Na coverage [50]. Across this coverage series the work function varies by about 3 eV as indicated in the figure. Interestingly, the observed chemical shift for the Na 1s ionization is very small in contrast to the shift observed in the Na KLL Auger spectra. A detailed analysis shows that the former is due to an accidental compensation of initial and final state effects of opposite signs. In the Auger spectra the final state effects become more important and allow a clear identification of three species formed in the process: Initially the adsorbed Na ions are positively charged (B), and after passing through the work-function minimum the signals due to metallic sodium, including the surface and bulk plasmons (A and D), appear and grow in intensity. Upon a slight increase in surface temperature Na_2O forms on the surface and at the same time NiO is reduced to metallic Ni which remains localized at the top of the NiO. This reaction is quite expected if we consider the bulk thermodynamics (see Table 2) of this system [56]. The reaction is exothermic by more than 170 kJ mol^{-1} . However, if we performed the same experiment for the system Na/ Cr_2O_3 in which case the reaction is exothermic by about 100 kJ mol^{-1} based on the bulk thermodynamic values, the corresponding redox reaction does not occur at the surface, as alluded to above.

An exchange of Na by Mg on the other hand induces the reaction which is not surprising considering the large exothermicity of the bulk reaction.

6. Adsorption on Metal Modified Oxide Surfaces

Adsorption on the metal modified systems discussed in the previous section is rather complex [57]. Therefore we review here some results on another system, where the reactivity of the supporting oxide is considerably reduced [6, 58 to 68]. In a series of detailed studies we have investigated the preparation and properties of a thin $\text{Al}_2\text{O}_3(111)$ film on a NiAl(110) substrate [61, 63]. Various metals have been deposited on this substrate, such as Ag, Pt, Pd, and Rh [58 to 66]. The different metals exhibit grossly different growth modes on this

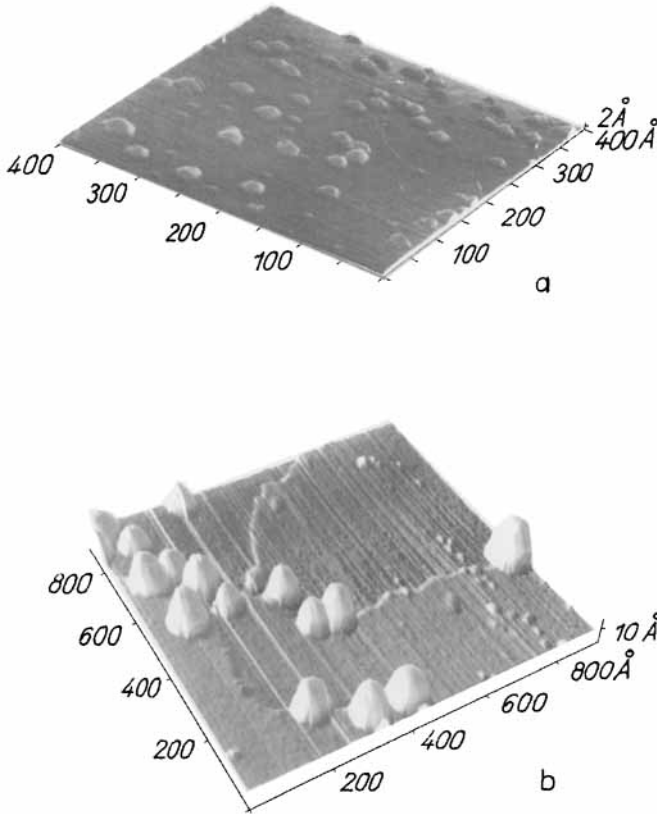


Fig. 20. a) Scanning tunneling micrographs of a Pt(0.5 Å)/Al₂O₃(111)/NiAl(110) preparation. The Pt deposits are shown as darker features. b) Scanning tunneling micrographs of a Ag(3 ML)/Al₂O₃(111)/NiAl(110) preparation. ($U = -0.6$ V; $I = 0.5$ nA). The Ag deposits are shown

substrate, depending on the strength of interaction of the metal with the substrate [6, 58, 59, 65]. Fig. 20 shows STM pictures of two metal deposits, namely Ag [58] and Pt [65]. While Ag weakly interacts with the substrate, and due to its high mobility at room temperature, coagulates at the steps of the Al₂O₃(111) film forming relatively large clusters, Pt interacts strongly with the substrate. For Pt we find relatively small clusters as revealed in the STM picture. We shall concentrate in the following on the Pt film.

The oxide film is imaged as a line pattern which is formed by an arrangement of hexagonal protrusions separated by about 10 Å. Pt is visible as small highly dispersed clusters as suggested by the SPA-LEED measurements. The measured height of the Pt clusters is between 1.5 Å for the small and 4 Å for the larger ones. Their diameter varies between 10 and 30 Å which leads us to estimate the number of Pt atoms per cluster to vary between 20 and 50 atoms.

The adsorption properties of the thin Pt film are in certain aspects very similar to the Pt(111) surface as is revealed via HREELS and TDS. An investigation of the chemical shift of the Pt/Al₂O₃ system measured via XPS reveals that the Pt is oxidized when it diffuses into the substrate [69]. One may speculate that the defect structure of the γ -Al₂O₃ substrate

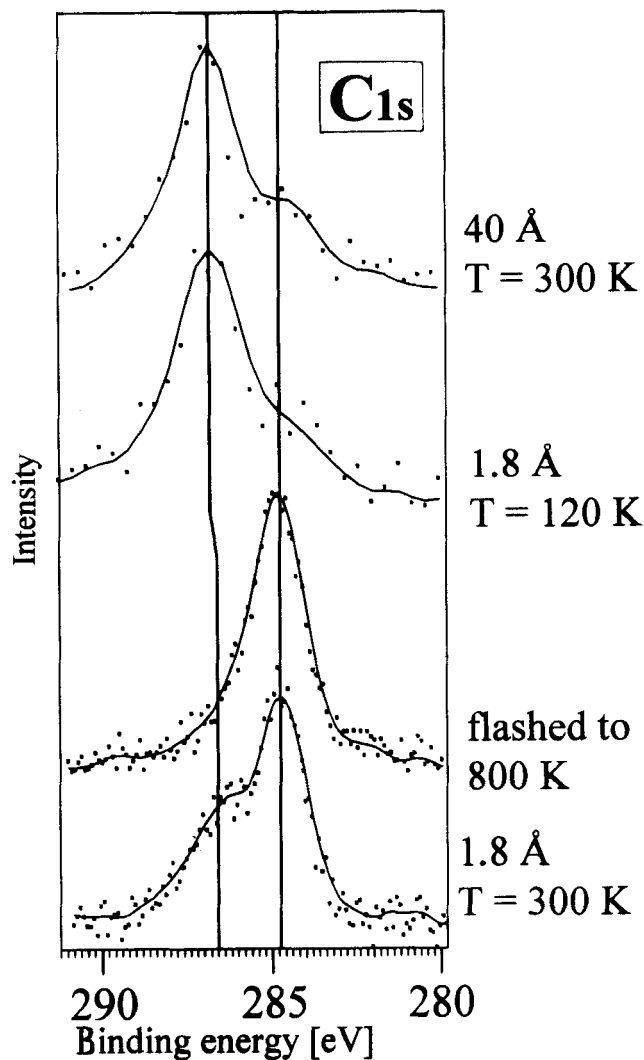


Fig. 21. C 1s XPS spectra of the system $\text{Pt}(x\text{\AA})/\text{Al}_2\text{O}_3(111)/\text{NiAl}(110)$ exposed to CO to saturation at various Pt coverages and substrate temperatures

helps to facilitate the diffusion of the relatively smaller Pt ions into the quasi-hexagonal top oxygen layer of the Al_2O_3 . Interestingly, the results on the model system may be compared with infrared spectra obtained for an Al_2O_3 powder sample impregnated with varying amounts of Pt. We have just begun to study reactions of CO with this Pt/ Al_2O_3 /NiAl system. Fig. 21 shows C 1s photoelectron spectra taken with monochromatized AlK_α excitation of a Pt overlayer ($\theta_{\text{Pt}} \approx 0.7$ ML) at various substrate temperatures. At low temperatures (90 K) we find a signal typical for molecularly adsorbed CO. It is, in fact, very similar to the spectrum recorded for a thick Pt film, shown for comparison. At 300 K, before desorption of CO from larger Pt aggregates occurs, we find a signal typical for adsorbed carbon at 284.8 eV in addition to the signal for molecularly adsorbed CO. The

molecular species desorbs above 400 K. The carbon signal remains even up to temperatures above 800 K. The cumulative information represents strong evidence that in contrast to CO on Pt single crystal surfaces CO dissociates at rather low temperatures, in particular below room temperature if this is not due to radiation induced effects. This finding may have consequences for reaction of CO with coadsorbed species on such systems if we can establish and finally prove the connection between particle site and reactivity [69].

7. Molecular Motion in Adsorbates

More and more the study of molecular motion shifts to the centre of interest in surface science. However, many of the standard surface science methods cover time scales that are much shorter than typical times required for molecular motion [70]. Typical time scales for molecular motion are of the order of 10^{-7} to 10^{-11} s. Electron spin resonance spectroscopy (ESR) is the spectroscopic technique operating in this time domain [71]. The first ESR experiment on a single crystal surface has been published by Baberschke and his group [72, 73]. However, they found that submonolayers of molecules on metal surfaces do not give rise to a detectable ESR signal because the coupling of the unpaired spin to the conduction electrons leads to very large line widths. In the present study we work with oxide surfaces with a very different electronic structure. Due to the localization of the electrons we can expect very different coupling leading to small line widths, especially if the coupling to the substrate is not too strong.

The experimental setup contains roughly two parts, namely the UHV chamber, which is located on top of the ESR magnet, and holds on the low end a gate valve which separates a typical ESR glass tube from the stainless steel chamber [70]. The sample mounted at the tip of an UHV manipulator may be moved between the UHV chamber and the final ESR measurement position within the glass tube. The UHV chamber is equipped with a TDS setup and a combined LEED/Auger optics. NO_2 has been used as a probe gas which was dosed through a capillary doser which establishes reproducible and pure NO_2 fluxes to the surface. The substrate is an Al_2O_3 film grown on a NiAl(110) alloy surface. Coverage calibration has been performed via TDS [74] as shown in Fig. 22. For small coverages a single desorption peak is found at 150 K which saturates at higher exposures. Then a second feature occurs with a peak temperature higher than the first one indicating three-dimensional growth of molecular aggregates (dimers) with higher intermolecular binding energy as compared with the binding energy between the individual molecule and the substrate. At very high coverage the desorption spectra show a rich structure interesting in itself but not to the present goal of studying dynamics. It should be stated, however, that the coverage calibration which is hard for such a complicated system has been established with another molecule (COS) which shows a growth mode where a full monolayer grows before the next one is populated. In Fig. 23 coverage dependent ESR spectra for the system $\text{NO}_2/\text{Al}_2\text{O}_3$ are shown. It is very reasonable to assume that the line width is dominated by dipolar intermolecular NO_2 interactions. Increasing the coverage leads to a closer packing of the molecules. Note that the surface temperature is 35 K, so that the molecules hit the surface and stick to it without diffusion.

If we anneal the surface at temperatures well below the desorption temperature and allow for diffusion the observed line widths dramatically decrease. On the other hand, if we annealed the surface above 100 K for longer times (a few minutes) the signal decreases completely. This is caused by the reaction of the paramagnetic NO_2 monomers to

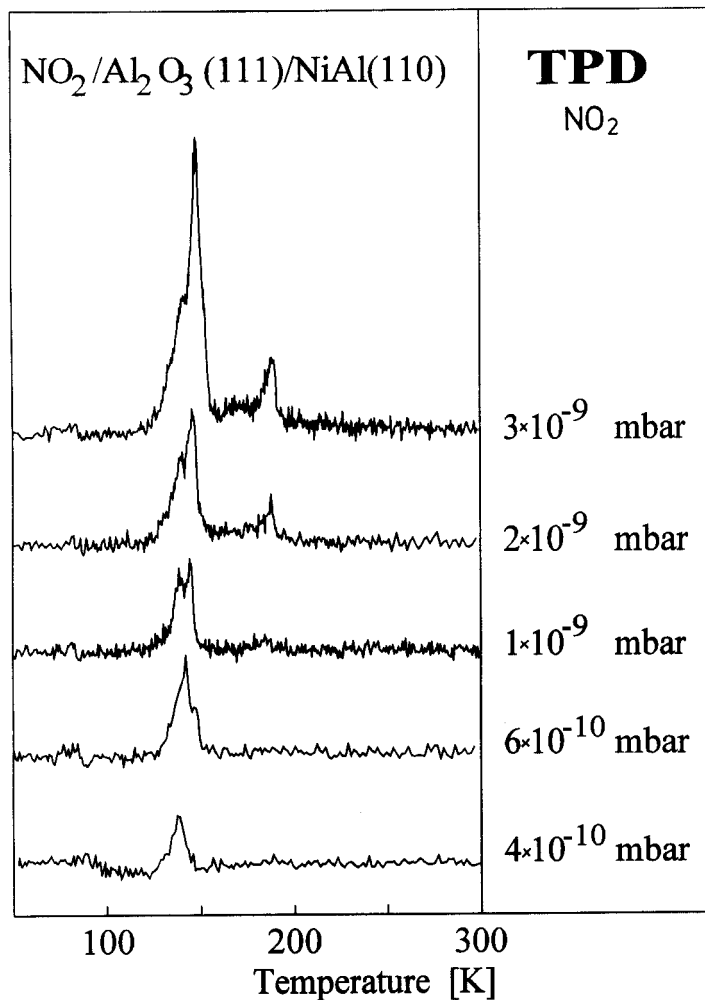


Fig. 22. Thermal desorption spectra of the system $\text{NO}_2/\text{Al}_2\text{O}_3(111)/\text{NiAl}(110)$ at various NO_2 coverages (1 mbar = 10^2 Pa)

diamagnetic N_2O_4 dimers. If the annealing procedure is repeated for moderate coverages for longer time intervals the decrease of line widths stops at a given value and only the line intensities decrease. At very low coverages this decrease in line width is not observed because the line width has reached its lowest limits already directly after adsorption. In this limiting case the dipolar interaction contribution is small compared to other contributions, e.g. those given by the interaction of the individual molecule with the substrate. The observed spectra have been simulated on the basis of two main considerations: One consideration is connected with the distribution of orientations in the sample, i.e. it could be either anisotropic or isotropic. The other consideration is concerned with the dynamics of motion of the molecules. To see this we resort to Fig. 24. ESR spectra of a submonolayer coverage are taken at different surface temperatures. The fits shown in the figure represent distributions of three-dimensionally randomly oriented and static molecules. It is quite obvious that the

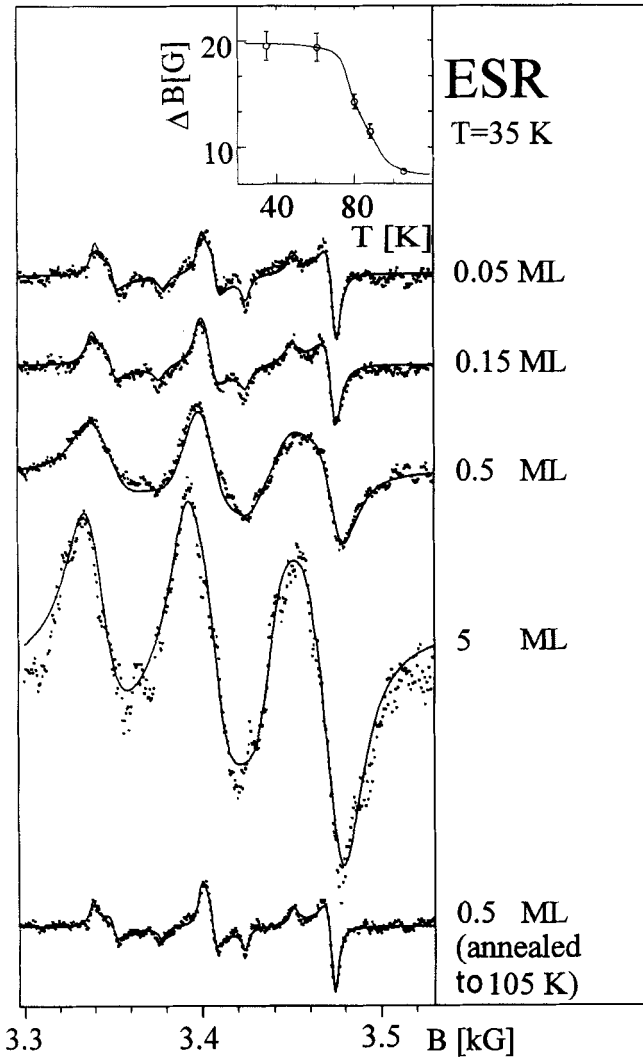


Fig. 23. UHV-ESR spectra of the system $\text{NO}_2/\text{Al}_2\text{O}_3(111)/\text{NiAl}(110)$ at various NO_2 coverages

fits are of better quality for the higher temperatures. This should not be the case if the deviations at lower temperatures corresponded to molecular motions, not taken into account by the fits. If, on the other hand, a molecular motion became unfrozen in the time window of the experiment the deviations from the static distribution should become larger with increasing temperature, eventually leading to motional narrowing of the lines. The simulation at highest temperature represents a static and isotropic distribution. The question is: What causes the deviations at lower temperatures? A possible answer is: A fraction of the molecules is oriented when they adsorb on the surface. This would explain the deviations. Upon raising the temperatures the contribution from the oriented molecules are removed from the distribution. This desorientation is an irreversible process. By cooling down to 35 K

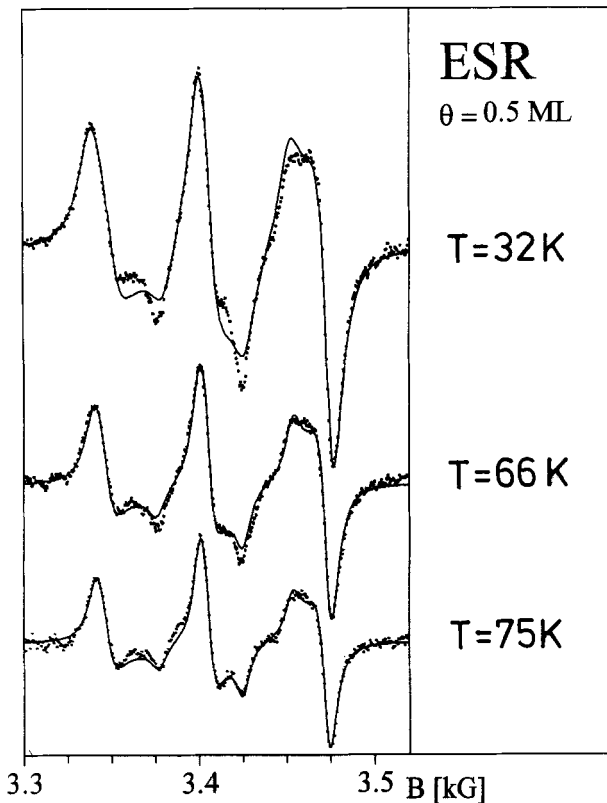


Fig. 24. UHV-ESR spectra of the system $\text{NO}_2/\text{Al}_2\text{O}_3(111)/\text{NiAl}(110)$ at the given coverage for various surface temperatures

after annealing the adsorbate, the three-dimensional randomly oriented and static distribution fits the spectrum quite well as is obvious from the lowest trace in Fig. 24.

Summarizing the results show the consequences of molecular motion: Diffusion is clearly visible through the dimerization of NO_2 monomers. However, no rotational motion of the molecules can be detected below 100 K in the time window of the experiment. Thus, the upper limit of the time window, 10^{-7} s, may be looked at as the upper limit for the rotational correlation time.

It is a task for the future to identify systems in which the onset of rotational motion of molecules or molecular fragments can be clearly identified. Self-organized films of long chain molecules, which are appropriately spin labelled [75] may be good candidates [76] for such observations.

Acknowledgements

A large number of colleagues, coworkers, and students have contributed to the work reviewed here. Some of them I would like to mention: B. Adam, Dr. K. Al-Shamery, Prof. P. Andresen (Bielefeld), Dr. M. Bäumer, Dr. B. Bartos, Dr. B. Baumeister, Dr. M. Beckendorf, M. Bender, I. Beauport, Dr. D. Cappus, B. Dillmann, D. Ehrlich, Dr. C. Fischer, Dr. H. Geisler, Dr. H. Hamann, K. Homann, Dr. M. Hassel, I. Hemmerich, Dr. G. Illing, Dr. R. Jaeger, U. Katter, Dr. J. Klinkmann, T. Klüner, Dr. H. Kühlenbeck, J. Libuda, Dr.

M. Menges, Dr. T. Mull, Prof. H. Neddermeyer (Halle), E. Neuhaus, Prof. M. Neumann (Osnabrück), Dr. G. Odörfer, Dr. T. Porwol, T. Risse, F. Rohr, N. Sauerwald, H. Schlienz, O. Seiferth, Prof. V. Staemmler, M. Wilde, Dr. F. Winkelmann, K. Wirth, Dr. J. Wambach, Dr. S. Wohlrab, Dr. C. Xu. I am very grateful to a number of agencies who have supported our work financially: Deutsche Forschungsgemeinschaft, Ministerium für Wissenschaft und Forschung des Landes Nordrhein-Westfalen, Bundesministerium für Forschung und Technologie, Europäische Gemeinschaft, and Fonds der Chemischen Industrie. Also, I would like to thank Studienstiftung des Deutschen Volkes for providing fellowships for some of my students over the years. Last but not least I would like to express my sincere thanks to the technical staff in our group: H. Böhm, G. Humme, H. Messing, T. Michels, H. Rayess, C. Risse, U. Uhde, and T. Wasmuth for their able assistance.

References

- [1] C. B. DUKE (Ed.), *Surface Science: The First Thirty Years*, North-Holland Publ. Co., Amsterdam 1994.
- [2] G. A. SOMORJAI, *Introduction to Surface Chemistry and Catalysis*, John Wiley & Sons, New York 1994.
- [3] G. ERTL and J. KÜPPERS, *Low Energy Electrons and Surface Chemistry*, Verlag Chemie, Weinheim 1989.
- [4] V. E. HENRICH and P. A. COX, *The Surface Science of Metal Oxides*, Cambridge University Press, 1994.
- [5] H.-J. FREUND and E. UMBACH (Ed.), *Springer Ser. Surface Sci.*, Vol. 33, 1993.
- [6] H.-J. FREUND, in: *Metal Ligand Interactions: Structure and Reactivity*, Ed. N. RUSSO and D. SALAHUB, NATO Advanced Study Institute, Kluwer Academic Press, Dordrecht, in the press.
- [7] M. BÄUMER, D. CAPPUS, H. KUHLENBECK, H.-J. FREUND, G. WILHELM, A. BRODDE, and H. NEDDERMEYER, *Surface Sci.* **253**, 116 (1991).
- [8] F. ROHR, K. WIRTH, J. LIBUDA, D. CAPPUS, M. BÄUMER, and H.-J. FREUND, *Surface Sci.* **315**, 2977 (1994).
- [9] K. MARRE and H. NEDDERMEYER, private communication (1992).
- [10] D. CAPPUS, C. XU, D. EHRLICH, B. DILLMANN, C. A. VENTRICE, K. AL-SHAMERY, H. KUHLENBECK, and H.-J. FREUND, *Chem. Phys.* **177**, 533 (1993).
- [11] D. CAPPUS, M. HASSEL, E. NEUHAUS, F. ROHR, and H.-J. FREUND, *Surface Sci.*, in the press.
- [12] A. FREITAG, V. STAEMMLER, D. CAPPUS, C. A. VENTRICE, K. AL-SHAMERY, H. KUHLENBECK, and H.-J. FREUND, *Chem. Phys. Letters* **210**, 10 (1993).
- [13] M. HASSEL, S. LÜTKEHOFF, H. KUHLENBECK, M. NEUMANN, A. FREITAG, V. STAEMMLER, and H.-J. FREUND, *Chem. Phys. Letters*, in the press.
- [14] P. S. BAGUS, G. PACCHIONI, and F. PARMIGIANI, *Chem. Phys. Letters* **207**, 569 (1993).
- [15] P. S. BAGUS, H.-J. FREUND, T. MINERVA, G. PACCHIONI, and F. PARMIGIANI, *Chem. Rev. Letters*, submitted.
- [16] C. XU, B. DILLMANN, H. KUHLENBECK, and H.-J. FREUND, *Phys. Rev. Letters* **67**, 3551 (1991).
- [17] C. XU, M. HASSEL, H. KUHLENBECK, and H.-J. FREUND, *Surface Sci.* **258**, 23 (1991).
- [18] H. KUHLENBECK, C. XU, B. DILLMANN, M. HASSEL, B. ADAM, D. EHRLICH, S. WOHLRAB, H.-J. FREUND, U. A. DITZINGER, H. NEDDERMEYER, M. NEUBER, and M. NEUMANN, *Ber. Bunsenges. phys. Chem.* **96**, 15 (1992).
- [19] C. A. VENTRICE, D. EHRLICH, E. L. GARFUNKEL, B. DILLMANN, D. HESKETT, and H.-J. FREUND, *Phys. Rev. B* **46**, 12892 (1992).
- [20] M. BENDER, D. EHRLICH, I. N. YAKOVKIN, F. ROHR, M. BÄUMER, H. KUHLENBECK, H.-J. FREUND, and V. STAEMMLER, *J. Phys. C*, submitted.
- [21] D. CAPPUS, M. MENGES, C. XU, D. EHRLICH, B. DILLMANN, C. A. VENTRICE, J. LIBUDA, M. BÄUMER, S. WOHLRAB, F. WINKELMANN, H. KUHLENBECK, and H.-J. FREUND, *J. Electron Spectroscopy related Phenomena* **68**, 347 (1994).
- [22] T. I. Y. ALLOS, R. R. BIRSS, M. R. PARKER, E. ELLIS, and D. W. JOHNSON, *Solid State Commun.* **24**, 129 (1977).

- [23] A. L. SCHAWLOW, D. L. WOOD, and A. M. CLOGSTON, *Phys. Rev. Letters* **3**, 271 (1959).
- [24] R. W. G. WYCKOFF, *Crystal Structures*, Vol. 1, 2nd ed., Interscience Publ., John Wiley & Sons, New York.
- [25] E. J. SAMUELSEN, M. T. HUTCHINGS, and G. SHIRANE, *Physica (Utrecht)* **48**, 13 (1970).
- [26] H. RIESEN and H. U. GÜDEL, *Mol. Phys.* **60**, 1221 (1987).
- [27] H.-J. FREUND and M. NEUMANN, *Appl. Phys. A* **47**, 3 (1988).
- [28] V. STAEMMLER, *Springer Ser. Surface Sci.*, **33**, 169 (1993).
- [29] G. PACCHIONI, K. M. NEYMAN, and N. RÖSCH, *J. Electron Spectroscopy related Phenomena* **69**, 13 (1994).
- [30] C. PISANI, R. DOVESI, R. NADA, and S. TAMIRO, *Surface Sci.* **216**, 267 (1989).
- [31] D. CAPPUS, J. KLINKMANN, H. KUHNENBECK, and H.-J. FREUND, *Surface Sci.* (1995), to be published.
- [32a] P. A. REDHEAD, *Vacuum* **12**, 203 (1962).
- [b] K. JACOBI, C. ASTALDI, P. GENG, and M. BERTOLO, *Surface Sci.* **223**, 569 (1989).
- [33] S. M. VESECKY, X. XU, and D. W. GOODMAN, *J. Vacuum Sci. Technol. A* **12**, 2114 (1994).
- M. C. WU, C. M. TRUONG, and D. W. GOODMAN, *J. phys. Chem.* **97**, 4182 (1993).
- C. M. TRUONG, M. C. WU, and D. W. GOODMAN, *J. Amer. Chem. Soc.* **115**, 3647 (1993).
- [34] H. KUHNENBECK, G. ODÖRFER, R. M. JAEGER, G. ILLING, M. MENGES, TH. MULL, H.-J. FREUND, M. PÖHLCHEN, V. STAEMMLER, S. WITZEL, C. SCHARFSCHWERDT, K. WENNEMANN, T. LIEDTKE, and M. NEUMANN, *Phys. Rev. B* **43**, 1969 (1991).
- H.-J. FREUND and E. UMBACH (Ed.), *Springer Ser. Surface Sci.*, Vol. 33, 1993.
- [35] M. PÖHLCHEN and V. STAEMMLER, *J. chem. Phys.* **97**, 2583 (1992).
- [36] G. PACCHIONI, G. COGLIANDRO, and P. S. BAGUS, *Surface Sci.* **225**, 344 (1991).
- G. PACCHIONI, T. MINERVA, and P. S. BAGUS, *Surface Sci.* **275**, 450 (1992).
- [37] G. PACCHIONI, *Surface Sci.* **281**, 257 (1993).
- G. PACCHIONI and P. S. BAGUS, *Springer Ser. Surface Sci.* **33**, 180 (1993).
- [38] K. M. NEYMAN and N. RÖSCH, *J. chem. Phys.* **168**, 267 (1992); *Surface Sci.* **297**, 223 (1993); *Chem. Phys.* **177**, 561 (1993).
- [39] M. A. NYGREN and L. G. M. PETERSSON, *J. Electron Spectroscopy related Phenomena* **69**, 43 (1994).
- [40] E. W. PLUMMER, T. GUSTAFSSON, W. GUDAT, and D. E. EASTMAN, *Phys. Rev. A* **15**, 2339 (1977).
- [41] C. L. ALLYN, T. GUSTAFSSON, and E. W. PLUMMER, *Chem. Phys. Letters* **47**, 127 (1977).
- [42] J. W. DAVENPORT, *Phys. Rev. Letters* **36**, 945 (1976); Thesis, University of Pennsylvania, 1976.
- [43] E. W. PLUMMER and W. EBERHARDT, *Adv. chem. Phys.* **49**, 533 (1982).
- [44] R. MIRANDA, K. WANDEL, D. RIEGER, and R. D. SCHNELL, *Surface Sci.* **139**, 430 (1984).
- [45] K. JACOBI, C. ASTALDI, P. GENG, and M. BERTOLO, *Surface Sci.* **223**, 569 (1989).
- [46] T. C. CHIANG, G. KAINDL, and D. E. EASTMAN, *Solid State Commun.* **36**, 25 (1980).
- [47] M. HASSEL and H.-J. FREUND, *Surface Sci.* **325**, 163 (1995).
- [48] H.-J. FREUND, in: *Handbook of Catalysis*, Ed. G. ERTL, H. KNÖZINGER, and H. WEITKAMP, Verlag Chemie, Weinheim, to be published.
- [49] H. P. BONZEL, A. M. BRADSHAW, and G. ERTL (Ed.), *Physics and Chemistry of Alkali Metal Adsorption*, *Materials Science Monographs*, Vol. 57, Elsevier Science Publishers BV, Amsterdam 1989.
- H. P. BONZEL, *Surface Sci. Rep.* **8**, 43 (1988).
- [50] M. BENDER, K. AL-SHAMERY, and H.-J. FREUND, *Langmuir* **10**, 3081 (1994).
- [51] D. EHRLICH, M. BENDER, I. N. YAKOVKIN, and H.-J. FREUND, unpublished.
- D. EHRLICH, Thesis, Ruhr-Universität Bochum, 1995.
- [52] C. KITTEL, *Introduction to Solid State Physics*, 4th ed., John Wiley & Sons, New York 1971.
- [53] H. RAETHER, in: *Ergebnisse der exakten Naturwissenschaften*, Vol. 38, 1965 (p. 84).
- [54] V. STAEMMLER, to be published.
- [55] I. YAKOVKIN, M. BENDER, and H.-J. FREUND, to be published.
- [56] *Handbook of Chemistry of Physics*, 52nd ed., Chemical Rubber Comp., Cleveland 1971/72.
- [57] M. BENDER, Diplomarbeit, Ruhr-Universität Bochum, 1993, unpublished.
- [58] H.-J. FREUND, B. DILLMANN, D. EHRLICH, M. HASSEL, R. M. JAEGER, H. KUHNENBECK, C. A. VENTRICE, F. WINKELMANN, S. WOHLRAB, C. XU, TH. BERTRAMS, A. BRODDE, H. NEDDERMEYER, *J. mol. Catalysis* **143**, 82 (1993).
- [59] F. WINKELMANN, S. WOHLRAB, J. LIBUDA, M. BÄUMER, D. CAPPUS, M. MENGES, K. AL-SHAMERY, H. KUHNENBECK, and H.-J. FREUND, *Surface Sci.* **307/309**, 1148 (1994).

- [60] S. WOHLRAB, F. WINKELMANN, H. KUHNENBECK, and H.-J. FREUND, Springer Proceedings in Physics, in the press.
- [61] R. M. JAEGER, H. KUHNENBECK, H.-J. FREUND, M. WUTTIG, W. HOFFMANN, R. FRANCHY, and H. IBACH, *Surface Sci.* **259**, 235 (1991).
- [62] J. LIBUDA, M. BÄUMER, and H.-J. FREUND, *J. Vacuum Sci. Technol. A* **12**, 2259 (1994).
- [63] J. LIBUDA, M. BÄUMER, H.-J. FREUND, TH. BERTRAMS, H. NEDDERMEYER, and K. MÜLLER, *Surface Sci.* **318**, 61 (1994).
- [64] J. LIBUDA, A. SANDELL, M. BÄUMER, and H.-J. FREUND, *Chem. Phys. Letters*, submitted.
- [65] T. BERTRAMS, F. WINKELMANN, TH. UTTICH, H.-J. FREUND, and H. NEDDERMEYER, *Surface Sci.*, in the press.
- [66] J. LIBUDA, Thesis, Ruhr-Universität Bochum, in preparation.
- [67] R. M. JAEGER, J. LIBUDA, M. BÄUMER, K. HOMANN, H. KUHNENBECK, and H.-J. FREUND, *J. Electron Spectroscopy related Phenomena* **64/65**, 217 (1993).
- [68] R. M. JAEGER, H. KUHNENBECK, and H.-J. FREUND, *Chem. Phys. Letters* **203**, 41 (1993).
- [69] F. WINKELMANN and H.-J. FREUND, to be published.
F. WINKELMANN, Thesis, Ruhr-Universität Bochum, 1995.
- [70] U. J. KATTER, H. SCHLIENZ, M. BECKENDORF, and H.-J. FREUND, *Ber. Bunsenges. phys. Chem.* **97**, 340 (1993).
- [71] C. P. POOLE, *Electron Spin Resonance*, Interscience Publishers, New York 1967.
C. P. KEIJZERS, E. J. REIJSE, and J. SCHMIDT, *Pulsed EPR: A New Field of Applications*, North-Holland Publ. Co., Amsterdam 1989.
- [72] M. ZOMACK and K. BABERSCHKE, *Surface Sci.* **178**, 618 (1986).
- [73] M. ZOMACK and K. BABERSCHKE, *Phys. Rev. B* **36**, 1756 (1987).
- [74] H. SCHLIENZ, M. BECKENDORF, U. KATTER, TH. RISSE, and H.-J. FREUND, *Phys. Rev. Letters* **74**, 761 (1995).
- [75] M. NILGES, M. SHOTANI, C. T. YU, G. BARKLEY, Y. KERA, and J. H. FREED, *J. chem. Phys.* **73**, 588 (1980).
- [76] TH. RISSE, Thesis, Ruhr-Universität Bochum, in preparation.